Fall 2018

Imaging the subsurface in eastern part of Lake Chesterfield using a combination of geophysical tools

Jiawei Li

IMAGING THE SUBSURFACE IN EASTERN PART OF LAKE CHESTERFIELD USING A COMBINATION OF GEOPHYSICAL TOOLS

by

JIAWEI LI

A THESIS

Presented to the faculty of the Graduate School of the

MISSOURI UNIVERSITY OF SCIENCE AND TECHNOLOGY

In Partial Fulfillment of the Requirements for the Degree

MASTER OF SCIENCE

in

GEOLOGICAL ENGINEERING

2018

Approved by:

Neil L. Anderson, Advisor
J. David Rogers
Evgeniy V. Torgashov

ABSTRACT

The Lake Chesterfield North Dam in Wildwood city, Missouri has been leaking, more or less continuously since the dam was constructed in 1986 despite mitigation efforts in 1988, 1994, 1995, 2004, and 2005. Neither the grouting efforts in 1988, 1994, 1995, 2004 or 2005, nor the placement and rehabilitation of an impervious clay liner in 2005 has solved the problem. Indeed, in June of 2017, the water level in Lake Chesterfield dropped at an alarmingly rapid rate.

Prior to authorizing additional mitigation work, the Lake Chesterfield Home Owners Association (LCHOA) decided to acquire geophysical data across the dry lake bed. The intent was to 1) map variable depth to the top of the rock; 2) identify karst features, including sinkholes and joints; 3) identify potential seepage pathway; and 4) determine soil and rock quality (based on resistivity and shear-wave velocity). It was believed that this information would help a geotechnical engineering firm determine the most appropriate mitigation plan.

During the survey, electrical resistivity tomography (ERT), multichannel analyses of surface wave (MASW) and spontaneous-potential (SP) geophysical tools were acquired across the dry lake bed. The interpretation of the data shows average depth to the top of rock is 10 ft. which consist with the test pit result by Geotechnology, Inc.; the rock above elevation of 600 ft. in Lake Chesterfield is mostly weathered/fractured limestone and can be described as poor-quality rock which could easily develop karst feature; three low resistivity zones at elevation below 600 ft. were found and could serve as vertical conduit of flowing groundwater; and two prominent low resistivity zones were found that could serve as potential seepage pathways through the North Dam.

ACKNOWLEDGEMENTS

I would like to express my appreciation and deep respect to my advisor, Dr. Neil L. Anderson, for his patient and gratuitous help during the period of this research. I would also like to thank my committee members, Dr. J. David Rogers and Dr. Evgeniy V. Torgashov, for their insightful comments. I also want to give my thanks to Dr. Evgeniy V. Torgashov, Abdullah Hadi, and James Hayes for their professional and wonderful cooperation during the field trip in Lake Chesterfield.

TABLE OF CONTENTS

LIST OF ILLUSTRATIONS

1. INTRODUCTION

The Lake Chesterfield North Dam in Wildwood city, Missouri has been leaking, continuously since the dam was constructed in 1986. The lake was grout was taken in 1988, 1994, 1995, 2004 and 2005 and still cannot solve the problem. Lake Chesterfield Home Owners Association (LCHOA) contacted Missouri University of Science and Technology (MS&T) in 2017 aim to find a permanent solution to the leaking issue.

The Lake Chesterfield was drained in fall 2017 for geophysical surveys. The Bara Geophysical Services crew spent total of 14 working days acquiring total of 12 ERT lines, 5 MASW sites, and 690 SP points' data. With almost 2 months data processing and interpretation, the result comes that Lake Chesterfield contains NNE/SSW and W/E trending solution widened joints across the whole lake and there probably have two large poor-quality rock area that allow the lake water seep beneath the dam and cause the leaking issue.

Based on the interpretation of the geophysical data, two suggestions were made to minimize the leakage. One is grouting, and the other is emplacement of liner. Both methods require drilling boreholes near the target area for further exploration and verification of the theory.

1.1. BACKGROUND

The Lake Chesterfield is situated in the western part of St. Louis, south of the Missouri River. It is the head of Caulks Creek, which is the tributary of the Missouri River. The coordinates of the lake are 90º 36' 40.53'' W, 38º 34'49.43''N using WGS84 projection system (Figure 1.1). Lake Chesterfield, including the dams, was designed by

Geotechnology, Inc. Construction started in 1986 and finished in 1987. The purpose was to provide stormwater detention and recreational zone for residents in the Lake Chesterfield Community. The North Dam is 700 ft. long, 90 ft. wide, and 32 ft. high; the South Dam is 200 ft. long, 65 ft. wide, and 15 ft. high. Both dams have driveway constructed on the top (Figure 1.2). Lake Chesterfield was divided into two parts by the South Dam. The northern section of Lake Chesterfield is approximately 2100 ft. long and 590 ft. wide (maximum). The size of the northern section of the lake is 22 acres when fully loaded (Figure 1.3). The southern section is much smaller at approximately 700 ft. long and 130 ft. wide (maximum).

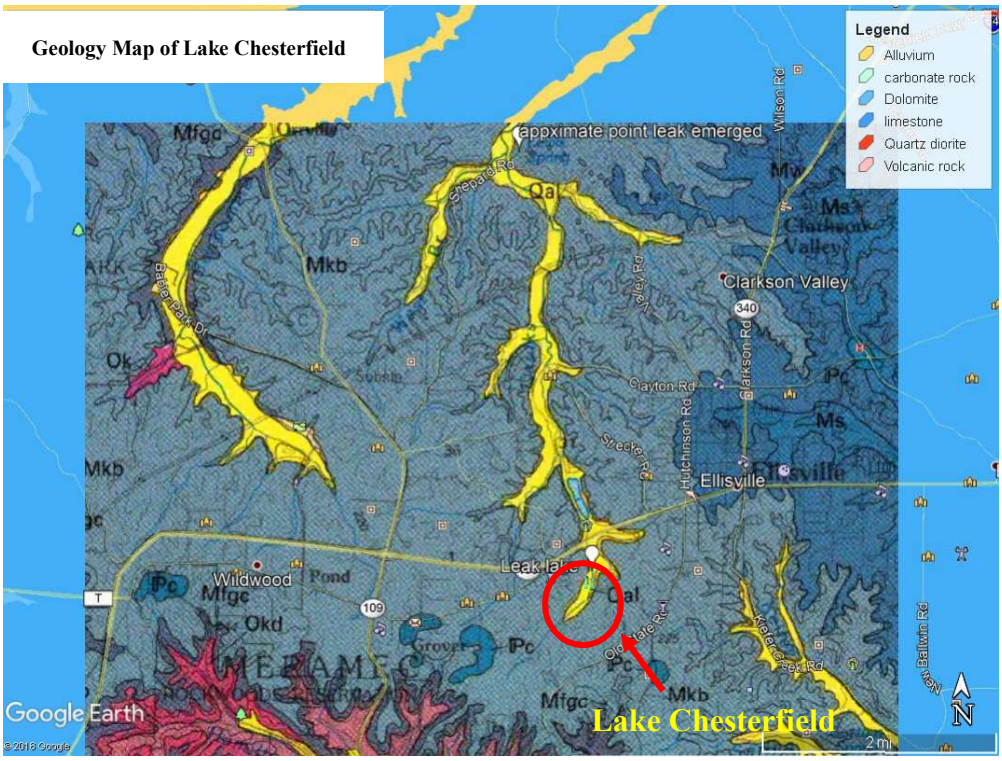

Figure 1.1. Lake Chesterfield is a part of a tributary of Missouri River. The red circle marks the location of the Lake Chesterfield. (Geology map by USGS, 1987).

According to the design report 'Subsurface Exploration – Dams and Lakes'. Geotechnology, Inc. used 17 test pits and 11 borings total for field exploration (Figure 1.4, 1.5, 1.6 and 1.7). They considered the potential seepage risk to be 3 to 6 in. per day and designed the compacted clay core, the cut-off trench and clay liner to reduce the quantity of seepage to 0.5 to 1 in. per day or less. The cut-off trench extends at least 5 ft. below clay core. The clay liner consists of at least two feet of compacted silty clay and extend up the bank slopes to two feet above normal water level.

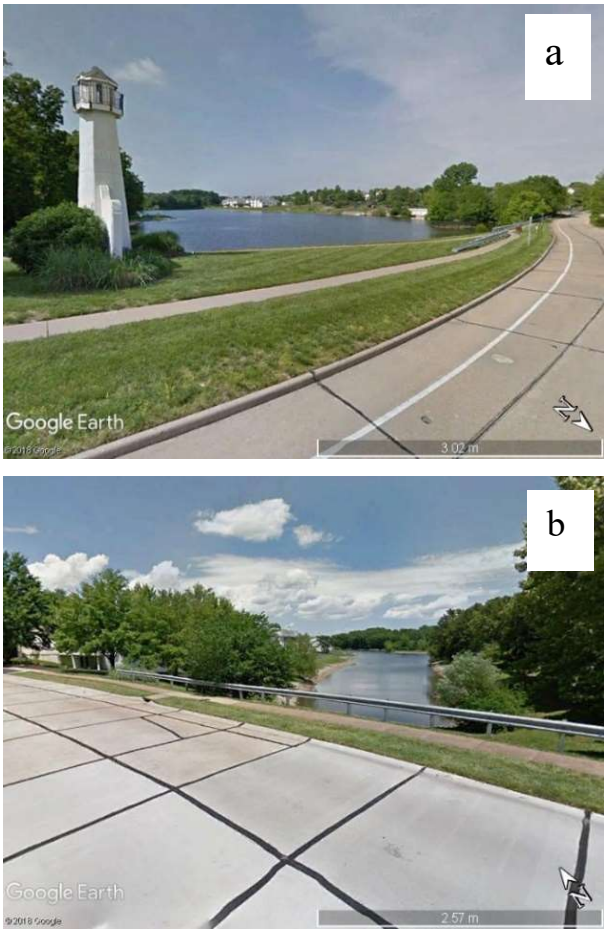

Figure 1.2. Lake Chesterfield Dams: (a) View of the North Dam. (b) View of the South Dam.

Figure 1.3. Map of Lake Chesterfield with two dams marked. Measuring based on Google Earth.

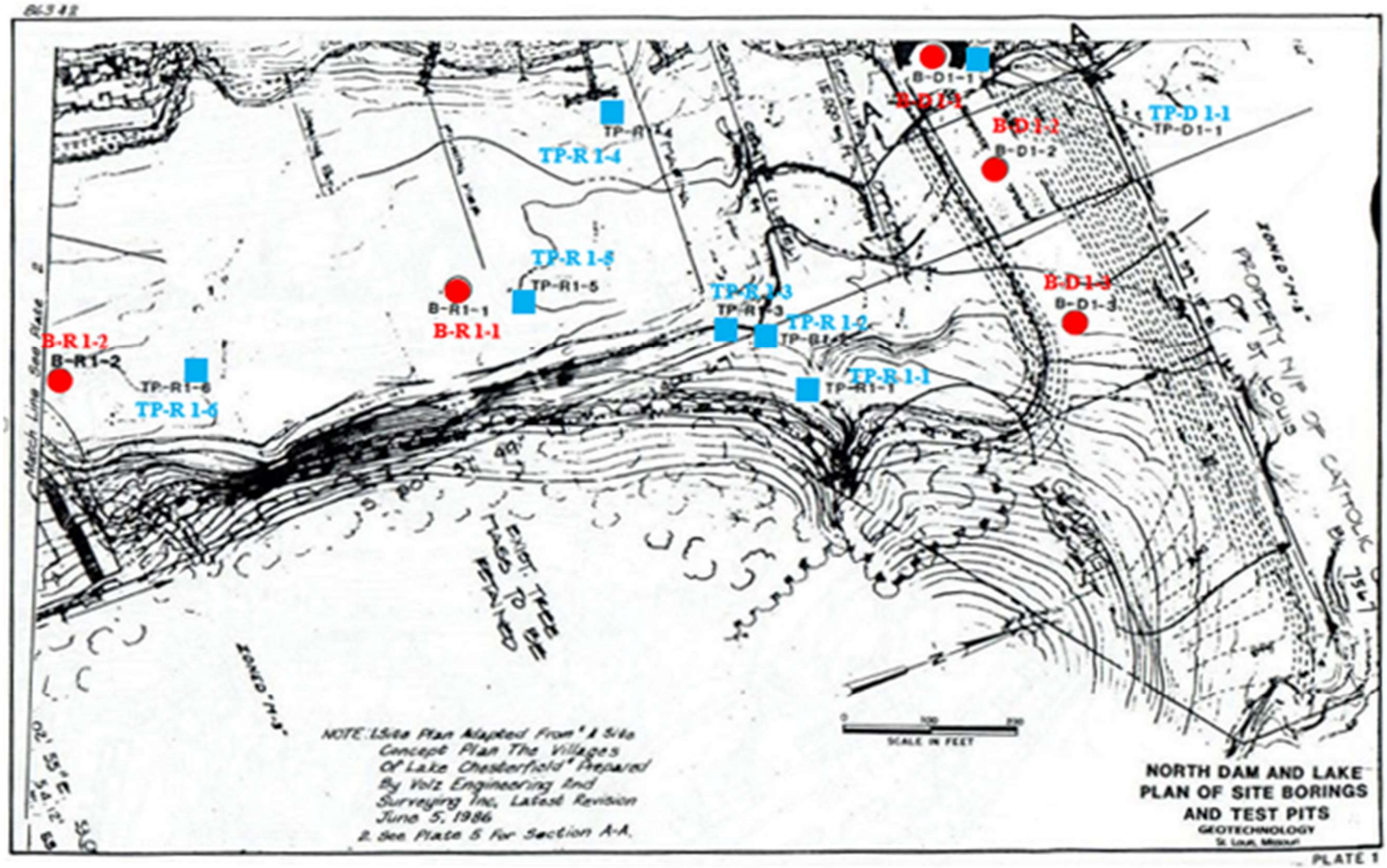

Figure 1.4. North Dam and lake plan of site borings and test pits. Red point marked as boring, blue square marked as test pits. Figure from dam design report generated by Geotechnology, Inc.

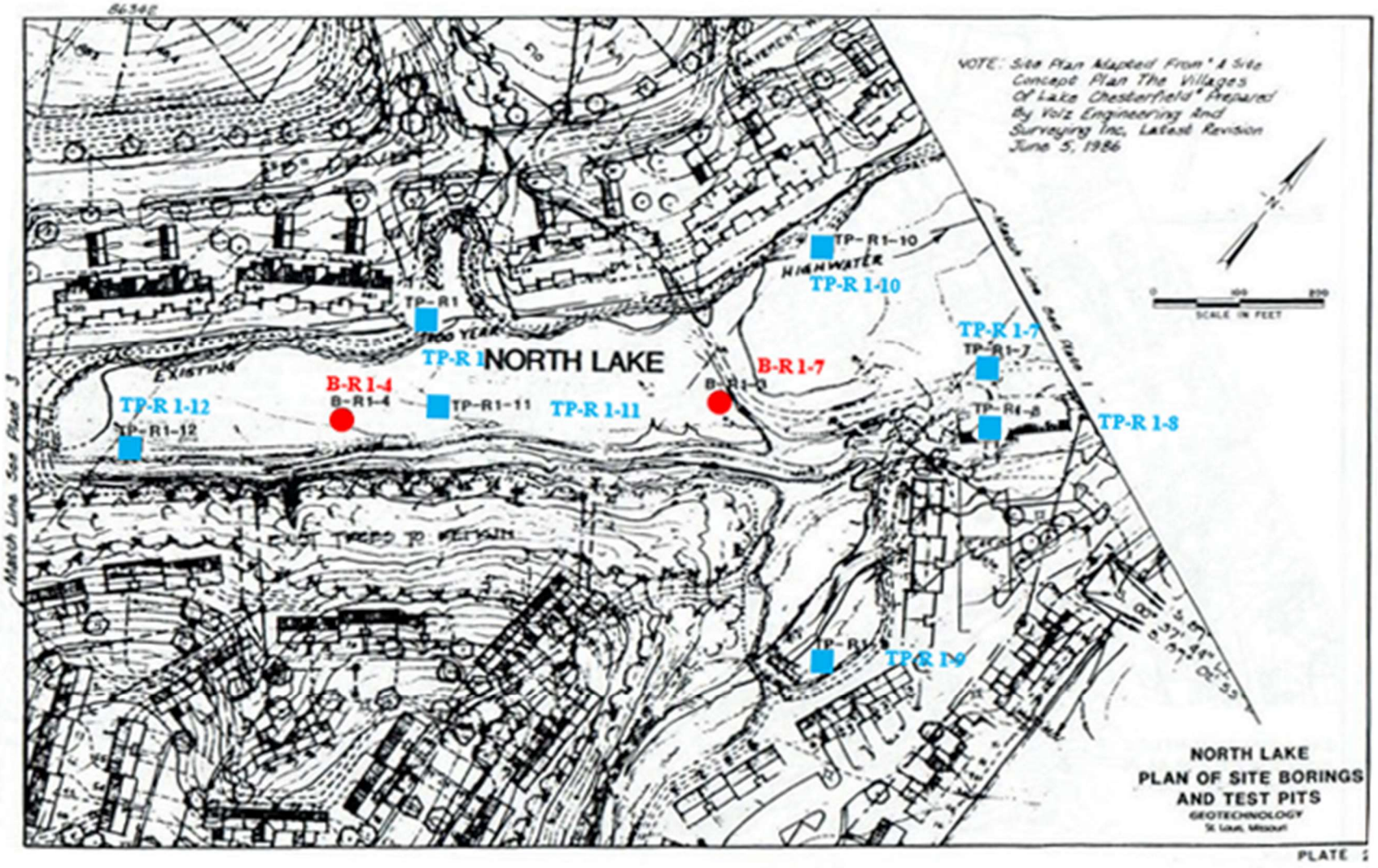

Figure 1.5. North Lake plan of site borings and test pits (Geotechnology, Inc., 1986).

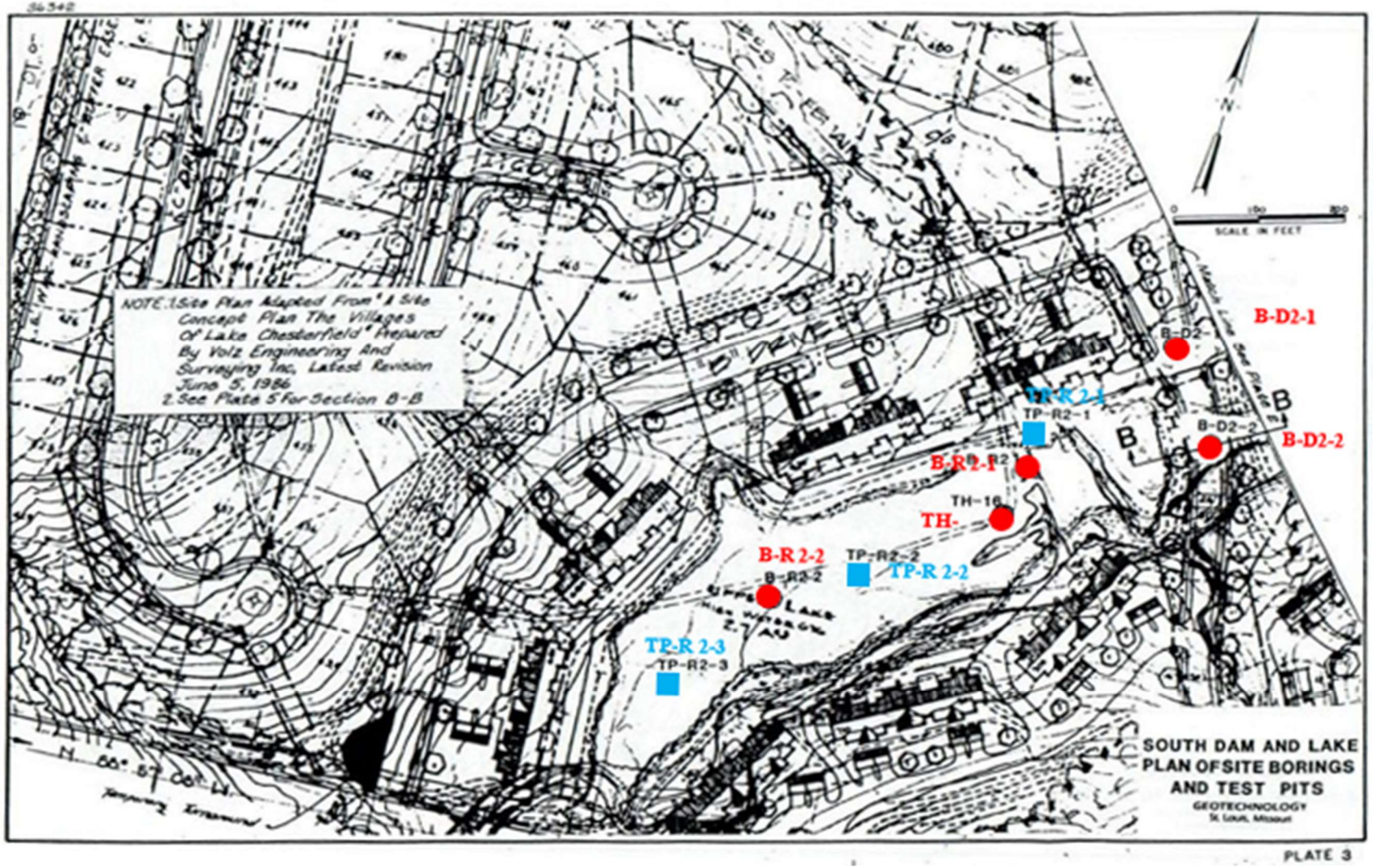

Figure 1.6. South Dam 'B-B' and lake plan of site borings and test pits (Geotechnology, Inc., 1986).

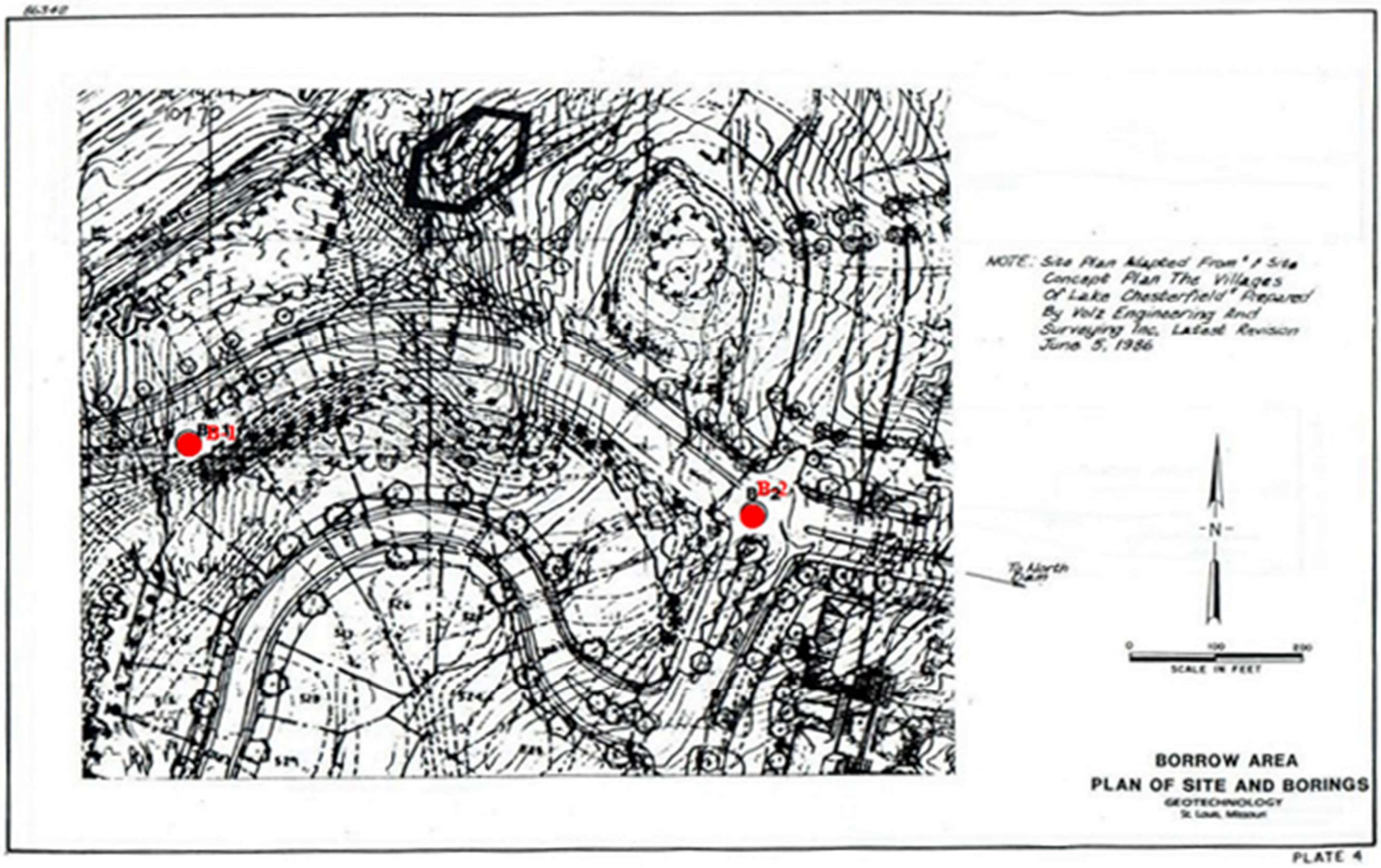

Figure 1.7. Borrow area plan of site and borings (Geotechnology, Inc., 1986) .

1.2. PREVIOUS ISSUES

Leaking of Lake Chesterfield has been recorded since the dam was built. According to the report 'Subsurface Exploration – Dams and Lakes' generated by Geotechnology, Inc., three sinkholes were developed during the construction period (Figure 1.8). One sinkhole was near the proposed tennis court location. The construction group found that the karst passageway underground was oriented NNE/SSW and treated it by placing several feet of 2 to 3-in. rock, capped with concrete, and backfilled with excavated soil. The second sinkhole was developed about 80 ft. east of the previous sinkhole area. The third sinkhole developed near the eastern shoreline. These two sinkholes were treated by excavated sinkhole down to intact rock and removing loose rock, then backfill the hole with excavated soil.

The first appearance of sinkholes after construction was reported in 1988. Three sinkholes opened from south to north and were grouted by Strata Services, Inc. In 1995, three sinkholes associated with a 12 ft. wide 160 ft. long subsidence trench were found along the eastern shoreline, and north of the previous sinkholes that developed in 1988. Approximately one thousand gallons per minute of water loss occurred. Strata Services, Inc. evidenced those leaks by water loss into the subgrade at point locations and slumping of the ground surface along lineaments that trended roughly N/S paralleling the eastern shore. 17 boreholes were drilled along the leakage area, a total of 4144 cubic ft. neat cement, and 1620 cubic ft. of sand-cement was injected into this area.

In 1996, four additional drill holes were made along the north, east, and south perimeter of the north sinkhole, and a total of 1036 cubic ft. neat-cement slurry and 324-

cubic ft. sand-cement slurry was injected into the sinkhole to significantly reduce the seepage rate.

In 2000, Strata Services, Inc. drilled five more boreholes on the east shoreline of the lake. A total of 796 cubic ft. of neat-cement group slurry and 486 cubic ft. of sand-cement grout slurry was injected into the subsurface to seal the leakage associated with subsidence features.

In May 2004, a small sinkhole formed at the south of the lake due to heavy rains. In June 2004, the main sinkhole formed northeast of the lake (Figure 1.8). The whole lake was drained in a few days. Water in the lake was dye-traced and emerged at Lewis Spring, which is located about 3.5 miles north of the lake. Shannon & Wilson, Inc. drilled five exploratory boreholes SW-1 to SW-5 on the North Dam with 40 ft. interval to determine the dam's condition. The water test of SW-1 and SW-2 was good in general. Test results of cores from the remaining holes determined 25 GPM or more, indicating the existence of leakage.

Shannon & Wilson, Inc. believed additional voids would develop on the eastern part of the lake, so Shannon & Wilson, Inc. acquired three ERT profiles for further exploration of subsurface (Figure 1.8). All three lines used dipole-dipole arrays, Line 1 was acquired in 7 ft. interval, Line 2 and 3 were acquired in 10 ft. interval. The survey completed on August 6, 2004. Data were processed into a 2-D resistivity model for analysis (Figure 1.9). The results determined bedrock of the western lake was in relatively good condition based on the 2-D model of line 3. Low resistivity zones appeared in the western part of line 1 and the northern part of line 2, which is near the

existing sinkhole. There were no significant eastwest trending pathways along line 2 and no concerns with solution features along the western shore.

After the drilling and geophysics survey, the excavation of the sinkhole began on September 7, 2004. Limestone was found at an approximate depth of 30 ft and a northeast clay-filled trending joint was found on September 22, 2004. The joint was 24 ft. long, 11 ft. wide, and at least 14 ft. deep. The joint continuously extends to northeast and finally entered a void oriented towards the northeast. The size of the void is approximately 6 ft. height and 3 ft. wide. Two smaller joints were found south of the primary joint with higher elevation and a few feet in length during the excavation. Water in two small joints can flow to the primary joint. After further excavation, limestone bedrock walls were exposed along the perimeter of a 30ft. by 40 ft. area with the exception of 15 ft. along the northern perimeter of the excavation. The backfill of flowable fill began on November 6, 2004, and finished on November 10, 2004, with a total of 289 cubic yards used to fill up joints and caves. The base of excavation was filled by several feet of imported high plastic clay, and the rest was using natural soil which consists of chert and limestone fragments. Shannon & Wilson, Inc. also investigated that the clay liner was missing along a large portion of the eastern shore, a total of 24 in. thick clay liner was placed by 8 in. thick lift each time and compacted by roller, then protected by geotextile fabric and riprap.

Strata Services, Inc. drilled 11 additional borings with intervals from 20 ft. to 40 ft. In August of 2004, 7 secondary grout holes with 10 ft. interval between primary holes were drilled in January and February of 2005 (Figure 1.8). According to Strata Services, Inc.'s grout report, the subsurface condition between borehole 1+60E and borehole

3+60E was unexpectedly deteriorated with 150 GPM or more leakage rate. Strata Services, Inc. reinforced the lake by injecting 7479 cubic ft. sand-cement pozzolan slurry into 14 drill holes between borehole 0+30E to borehole 1+60E and let Shannon & Wilson, Inc. take care of the sinkhole remediation since condition of subsurface situated east of borehole 1+60E were not applicable for grouting methods anymore. All grouting was finished in August 2005 but did not effectively seal the lake. The water testing shows only 40 percent decrease in the permeability of the subgrade, but seepage rate was reduced significantly. Strata services, Inc. recommended additional 13 intermediate holes with 5-ft. intervals to verify full closure.

1.3. CURRENT ISSUE

According to the Lake Chesterfield Homeowners Association (LCHOA), the leaking issue became worse since 2005. In June 2017 the water level dropped multiple inches per day. LCHOA wants to find a permanent solution to the leaking issue and contacted Missouri University of Science and Technology for help. The lake was drained for the exploration geophysical survey.

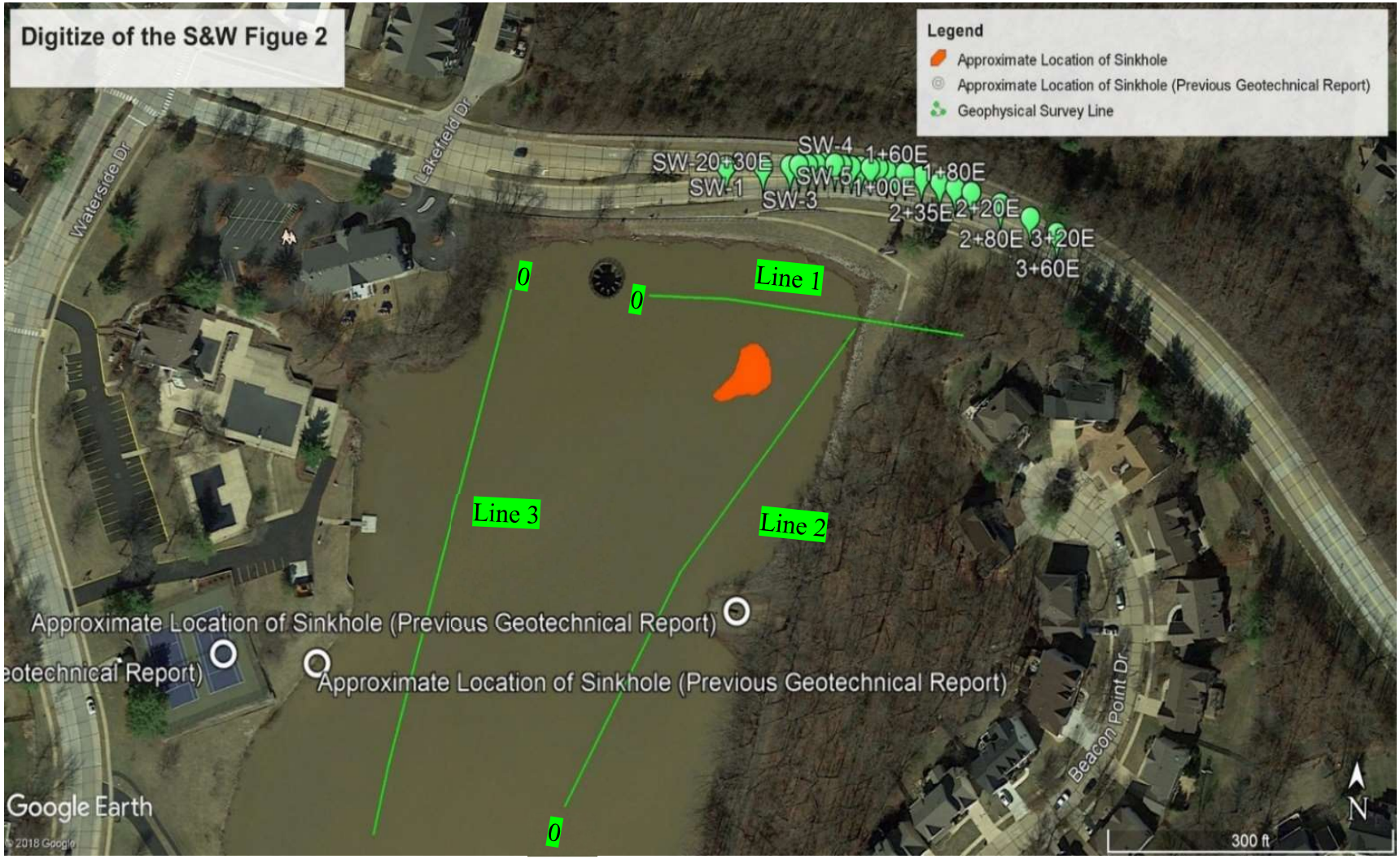

Figure 1.8. Digitize version of the Shannon & Wilson's surveys. The green line represents ERT traverses; the orange area represents the location of the sinkhole that opened on June 4, 2004.

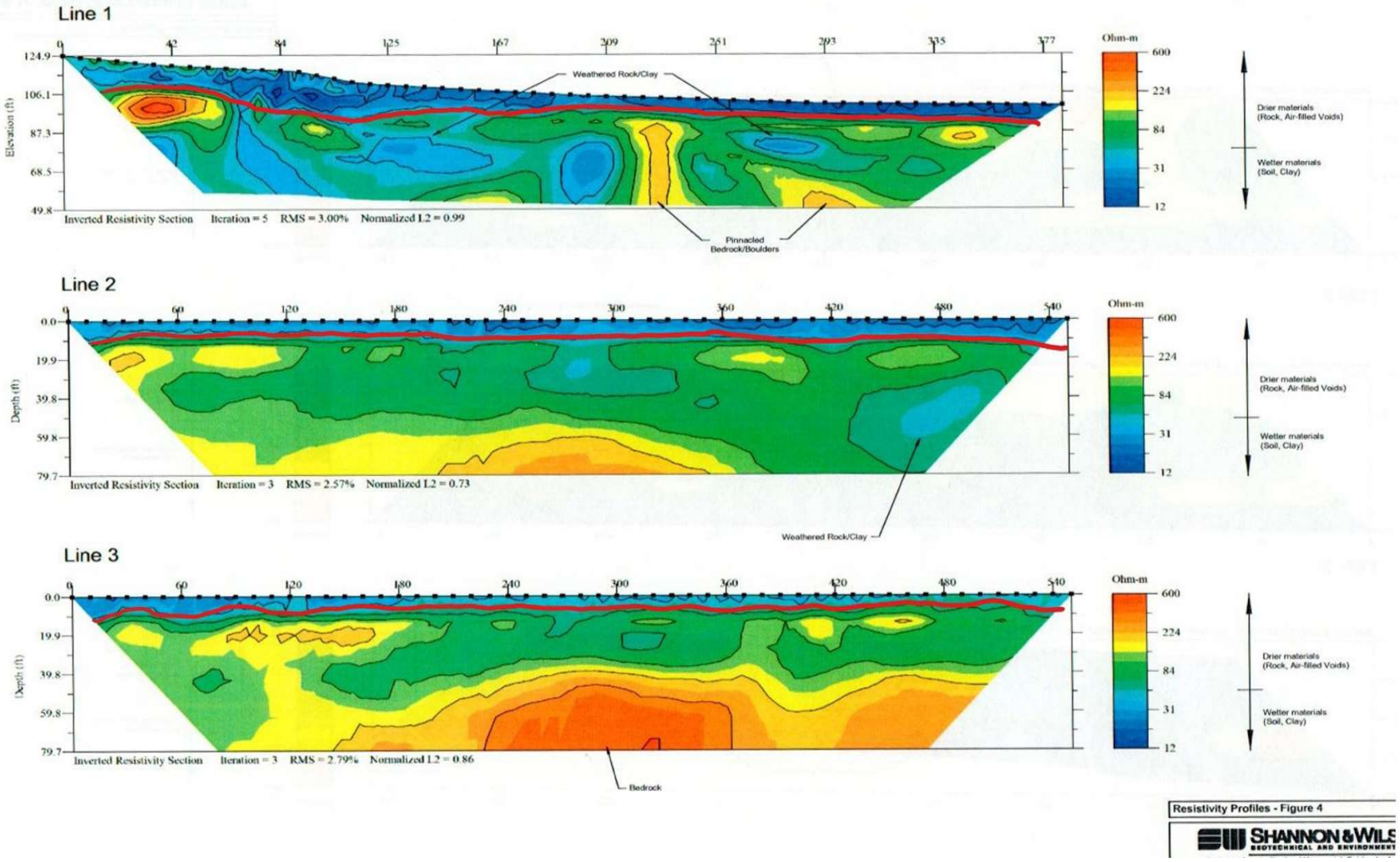

Figure 1.9. ERT 2-D model generated by Shannon & Wilson, Inc., from 'Lake Chesterfield Exploration and Repair Summary Report' Figure 4. Red line represents interpreted top of rock. Data are consistent with the ERT data acquire.

2. CURRENT GEOPHYSICAL INVESTIGATION

This research mainly focuses on the eastern part of the Lake Chesterfield. Twelve new ERT survey lines named ERT 1-7 and ERT A-E were set to associate with previous surveys for better conclude the subsurface features (Figure 2.1). The ERT survey used dipole-dipole arrays with a 5 ft. electrode interval. Five multi-channel analysis of surface waves (MASW) survey locations were marked as MASW 1-5 on the eastern part of the lake. MASW using the active 24-channel MASW method with 2.5 ft. electrode interval. Self-potential (SP) data was acquired with 20 ft. interval in 14 lines (first two lines using 5 ft. interval) ERT data were acquired using 168-channel SuperSting R8 developed by AGI, and data processing using Res2DInv inversion software by Geotomo. Visualization was completed using Surfer software by Golden software.

ERT, MASW, and SP were employed together in order to characterize the subsurface feature effectively. Objectives of this study were as follow:

1) Map variable depth to the top of the rock;

2) Identify karst features, including sinkholes and joints;

3) Identify potential seepage pathways;

4) Determine soil and rock quality (based on resistivity and shear-wave velocity).

The LCHOA believed these data would help future geotechnical engineering company to develop the plan to minimize the seepage problem.

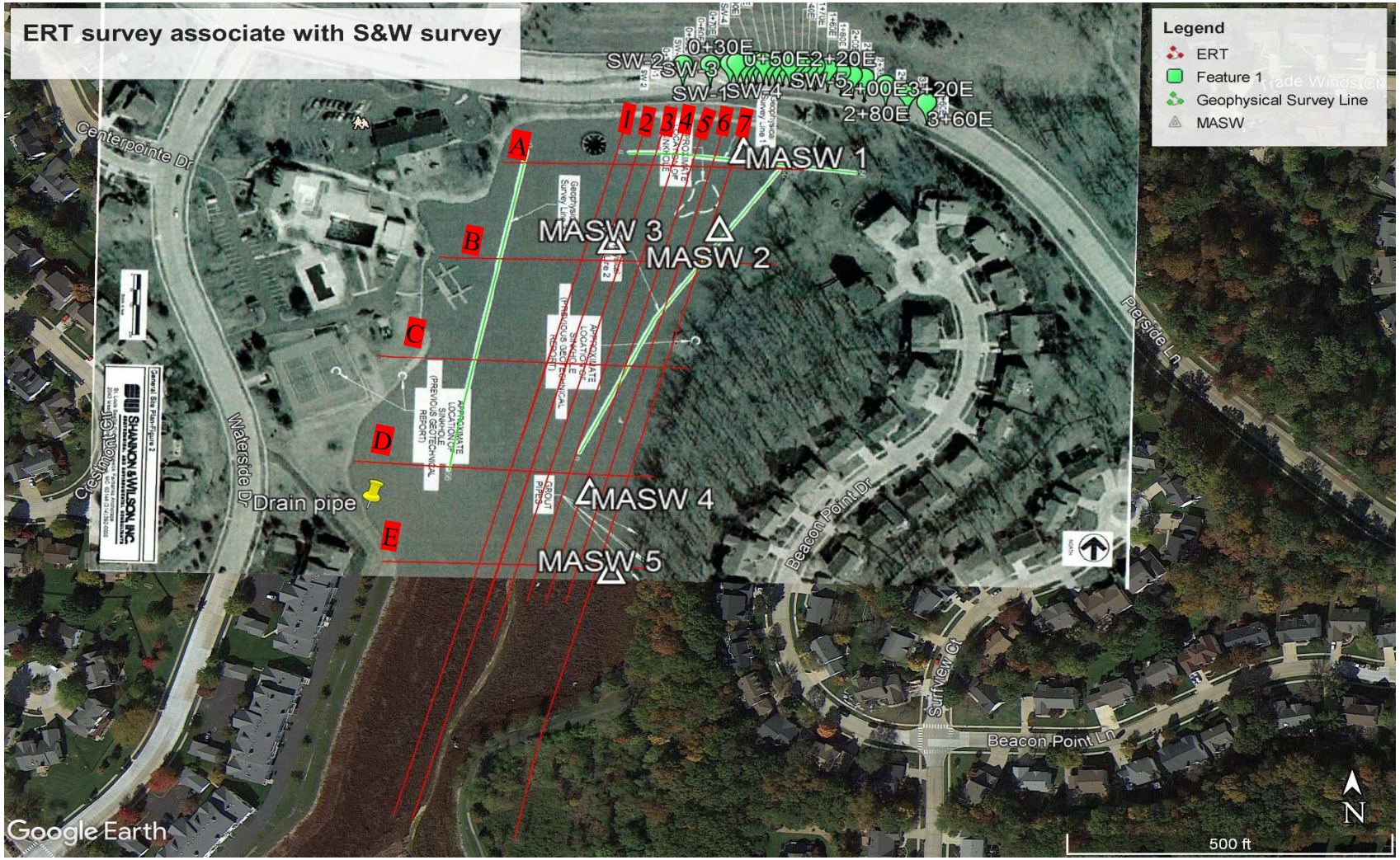

Figure 2.1. ERT and MASW field investigations and digitization of Shannon & Wilson, Inc. 2005 'Lake Chesterfield Exploration and Repair Summary Report' Figure 2. Red lines represent ERT lines required in 2018.

3. GEOLOGIC SETTING

Lake Chesterfield situated in Wildwood, Missouri. It is a tributary of Missouri River, which is the level 1 stream according to Strahler Stream Order.

3.1. GEOGRAPHY OF WILDWOOD

Wildwood is a city that located in western St. Louis, Missouri (Figure 3.1). It is bound to the north by Chesterfield, to the east by Clarkson Valley, to the south by Eureka and Pacific, and to the west by Franklin. The total area of Wildwood is 67.08 square miles. It is situated at the edge of the Ozarks Highlands physiographic region and in a warm/humid continental climate region (Figure 3.2).

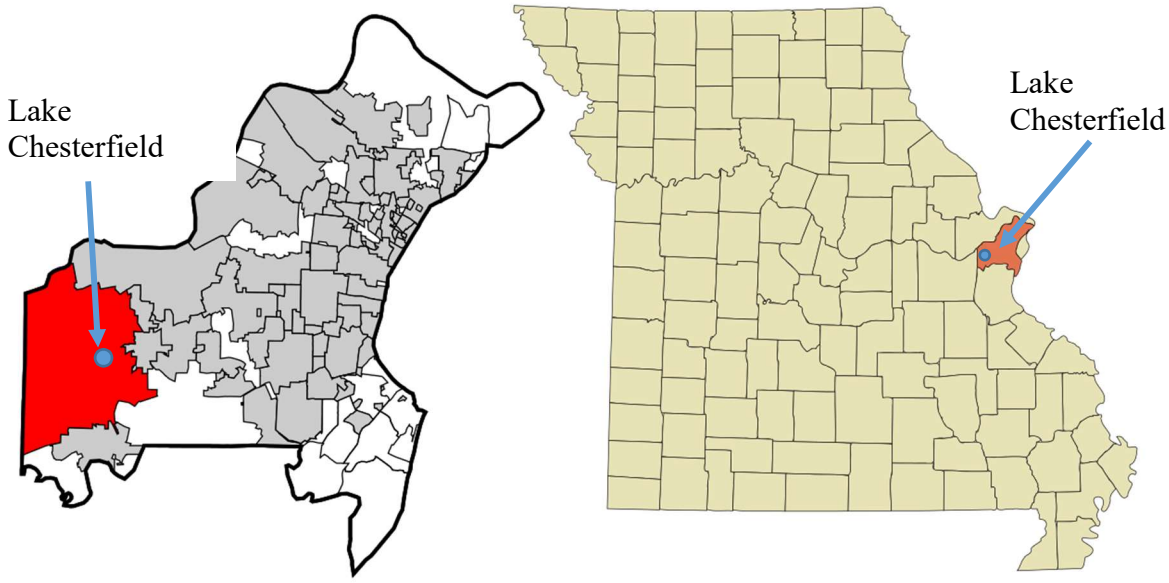

Figure 3.1. Location map of the study area in Wildwood City, Missouri (Arkyan, 2007).

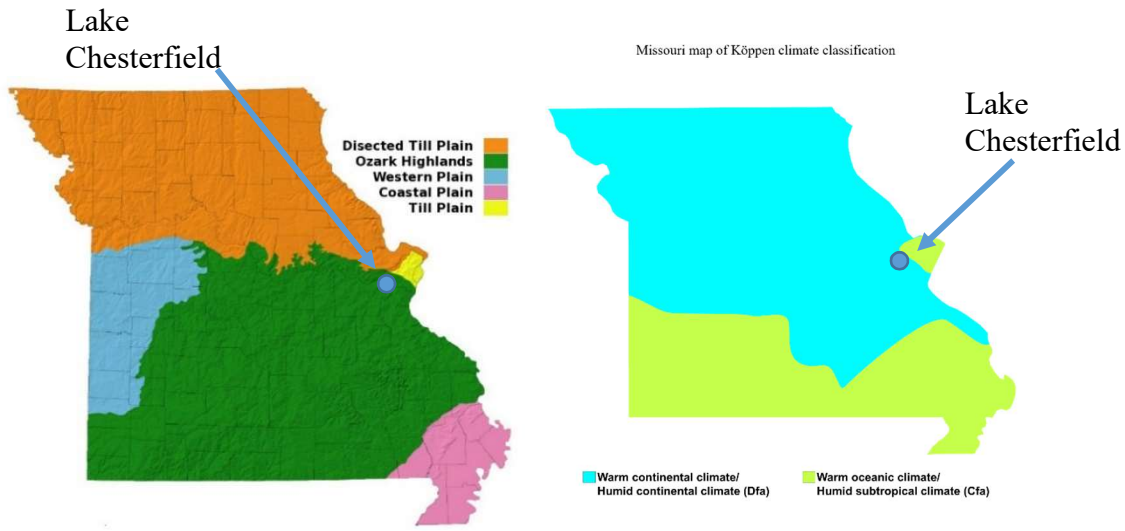

Figure 3.2. Missouri physiographic region (left) and climate map (right) (kbh3rd, 2009; and Ali Zifan, 2016).

3.2. STRATIGRAPHY OF STUDY SITE

According to the United States Geological Survey (USGS) database, majority type of bedrock in Missouri is limestone and dolomite (Figure 3.3). The two nearest well log data provided by Missouri Department of Natural Resources (MODNR) identified the average appearance of limestone and dolomite at approximately 50 ft.; log ID 024175 is 0.55 miles away from the study area and log ID 023103 is 0.42 miles away from the study area (Figure 3.4). According to the dam design report from Geotechnology, Inc., the stratigraphy in Lake Chesterfield is low plasticity silty clay underlain by clay with embedded chert gravel to clayey gravel on top stratum. Shannon & Wilson, Inc. drilled five exploration wells SW-1 to SW-5 on 25 ft. high earth fill dam, cores from wells identified reddish-brown fat clay and silt with chert fragments from average 25 to 48 ft. depth and highly weathered limestone and dolomite with white to light gray chert layers, and shale filled stylistic partings fragments from average 48 to 73 ft. depth underground.

In Short, the stratigraphy near Lake Chesterfield can be described as limestone and dolomite overlaied by clay, silt and highly weathered limestone. The thickness of top soil and weathered rock is approximately 50 ft.

3.3. KARST TERRAIN IN MISSOURI

In the United States, all 50 states contain rocks with potential for karst development, and about 18 percent of the United States are underlain by soluble rocks having karst features or the potential for development of karst features (David & Daniel, 2014). According to David's map, there are three-fourths of Missouri covered with carbonate rock (Figure 3.5).

3.3.1. Philosophy. Karst features are mostly formed by dissolution of soluble rocks, such as limestone, dolomite. The dissolution process can be expressed by the following chemical reactions:

$$CO_2+H_2O \rightleftharpoons H_2CO_3$$

$$H_2CO_3 \rightleftharpoons H^+ + HCO_3^-$$

$$H^+ + CaCO_3 \rightleftharpoons HCO_3^- + Ca^{2+}$$

Carbon dioxide in the atmosphere dissolves in surface water to form carbonic acid. The carbonic acid reacts with carbonate rock to form soluble ions that lead to the formation of sinkholes. Karst features are always associated with frequent caves and sinkholes in the subsurface. From the database provided by Missouri Department of Natural Resources (MODNR), the Geological Survey Program has verified 15,981 sinkholes in Missouri (Figure 3.6) and are frequently presented in St Louis city.

3.3.2. Sinkhole Formation. There are three types of sinkholes that formed in karst terrain, including solution sinkhole, subsidence sinkhole, and collapse sinkhole.

Solution sinkholes, also called solution dolines, are formed where surface water and/or soil water dissolves bedrock at the surface or rockhead as it flows toward points where it can sink into the fissured and/or cavernous ground (Waltham, 2007) (Figure 3.7-a). Solution sinkholes frequently develop in low-lying area or lakes. They are long-term landform and mainly consist of karst terrain. The size of solution sinkholes can vary from 10 to 1000 m. Sinkholes that form close to each other can combine during expansion over time.

Subsidence sinkhole is the most widespread geohazard in karst of soluble rocks. Sandy soil on the top of the carbonate bedrock will easily sink into void in the subsurface. Because sandy soil is not compact enough, when lower layer of soil sink into the subsurface void, upper layer of soil will slump due to the soil lose, which subsidence sinkhole will form (Figure 3.7-b). Subsidence sinkholes cause many of the major problems for engineering works on cavernous karst and account for the great majority of sinkhole damage to roads and buildings (Waltham, 2007). The size of subsidence sinkholes can vary from 1m to 100 m in diameter.

Collapse sinkholes are not common. They are defined by fracturing, breakdown, and collapse of unsupported bedrock slabs, beams, and arches that are left around dissolution cavities in karst (Waltham, 2007). This kind of sinkhole will develop when the topsoil contains high percentage of clay or silt. When erosion occurs on bedrock, the top stratum will keep original shape until it is thin enough that it could not offset self-gravity, will resulting in collapse (Figure 3.7-c). The size of a collapse sinkhole can vary but is rarely over 100 m in diameter.

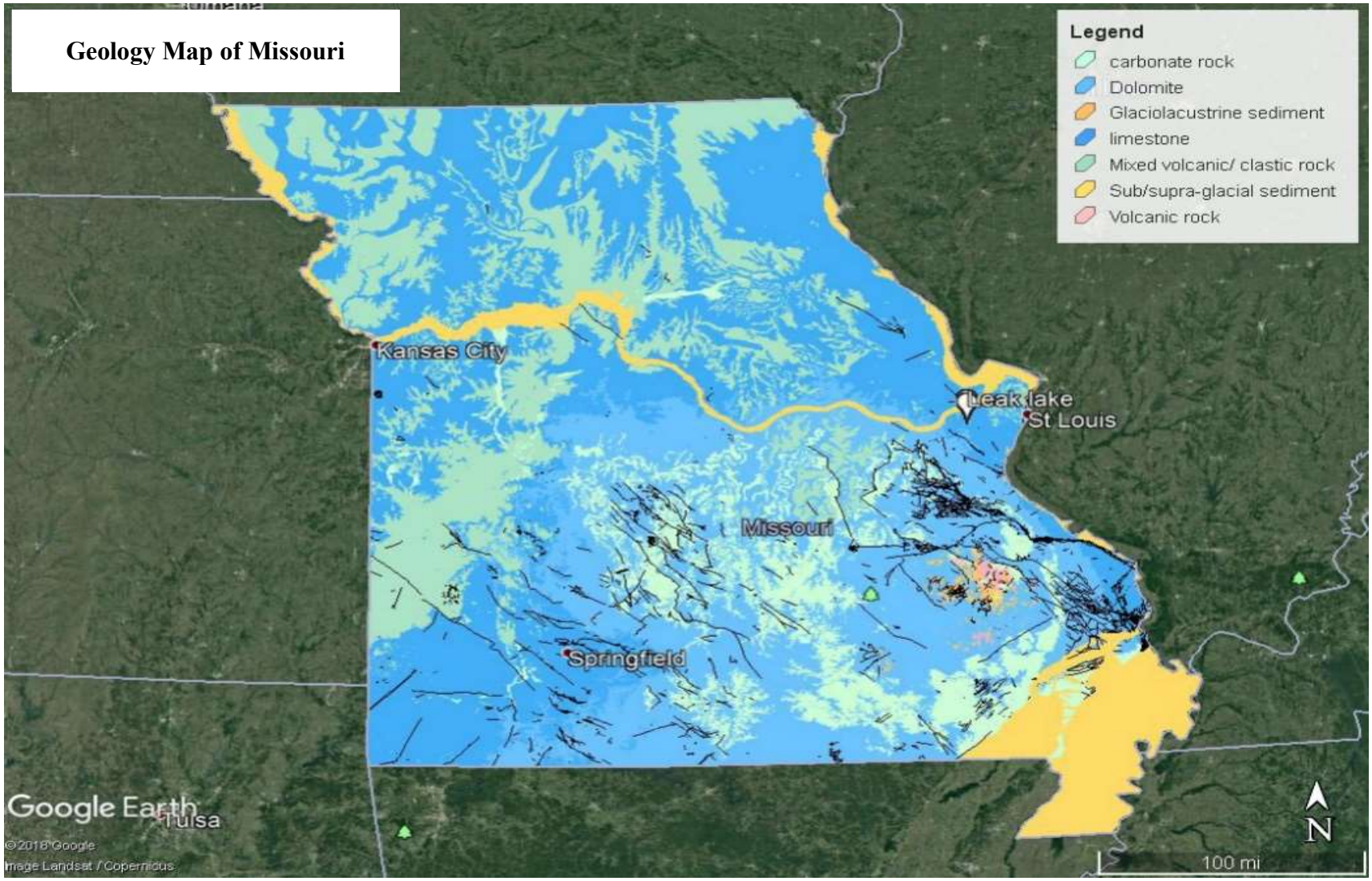

Figure 3.3. The geology map of Missouri.

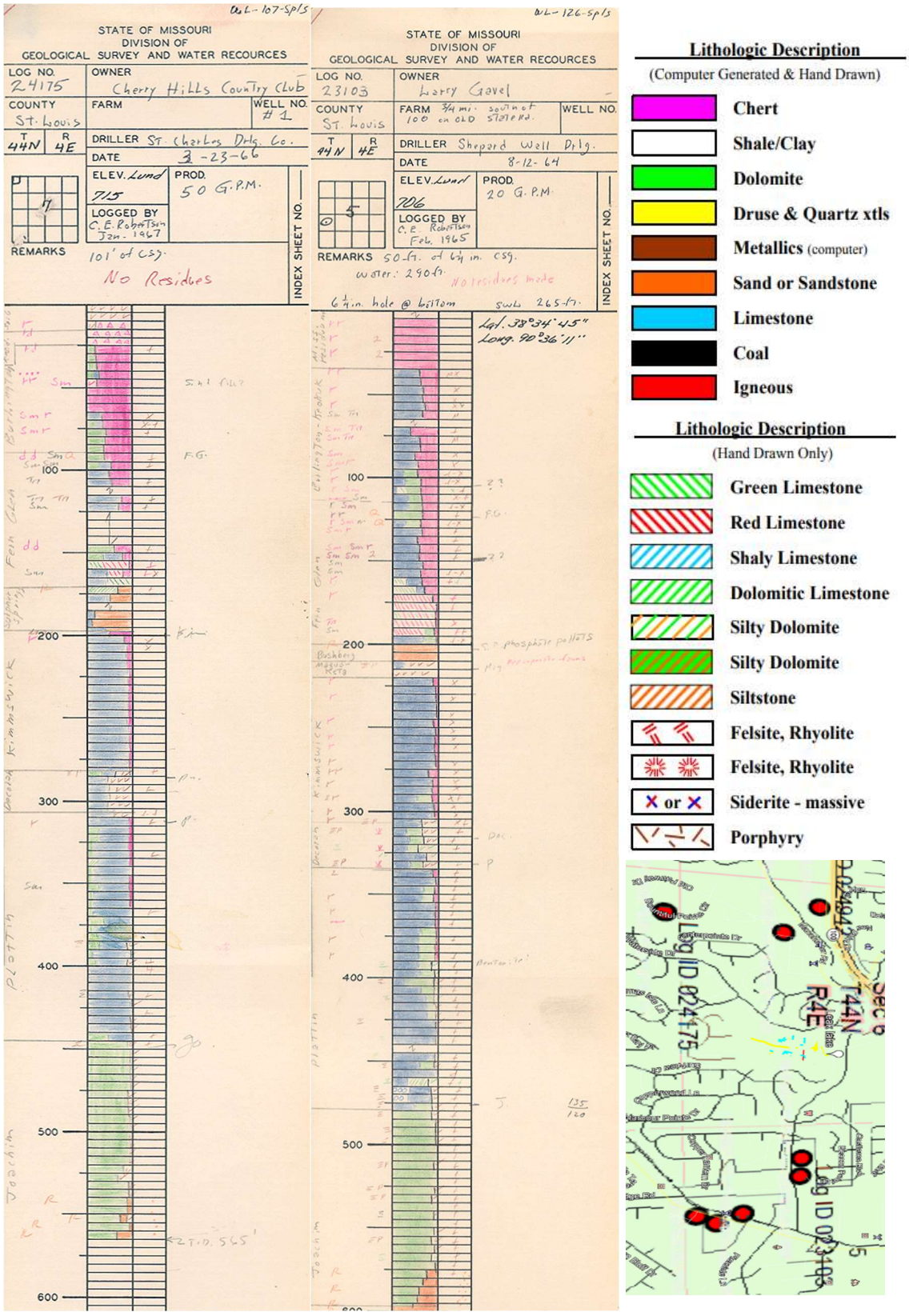

Figure 3.4. Well log 024175 (left) and well log 023173 (right) (MODNR, 2018).

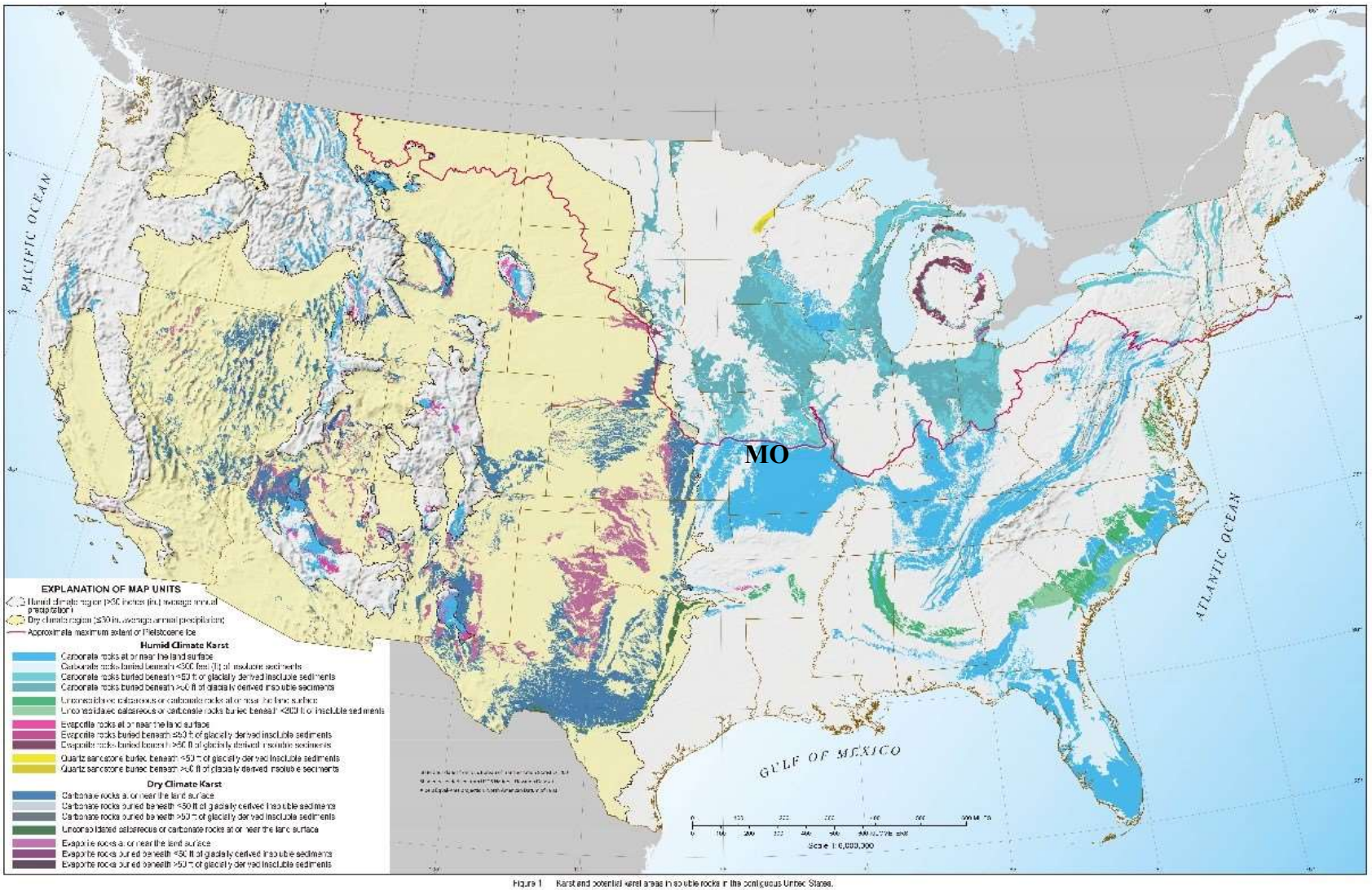

Figure 3.5. US potential karst development map (Weary and Doctor, 2014).

Figure 3.6. Verified sinkholes in Missouri (MODNR, 2018).

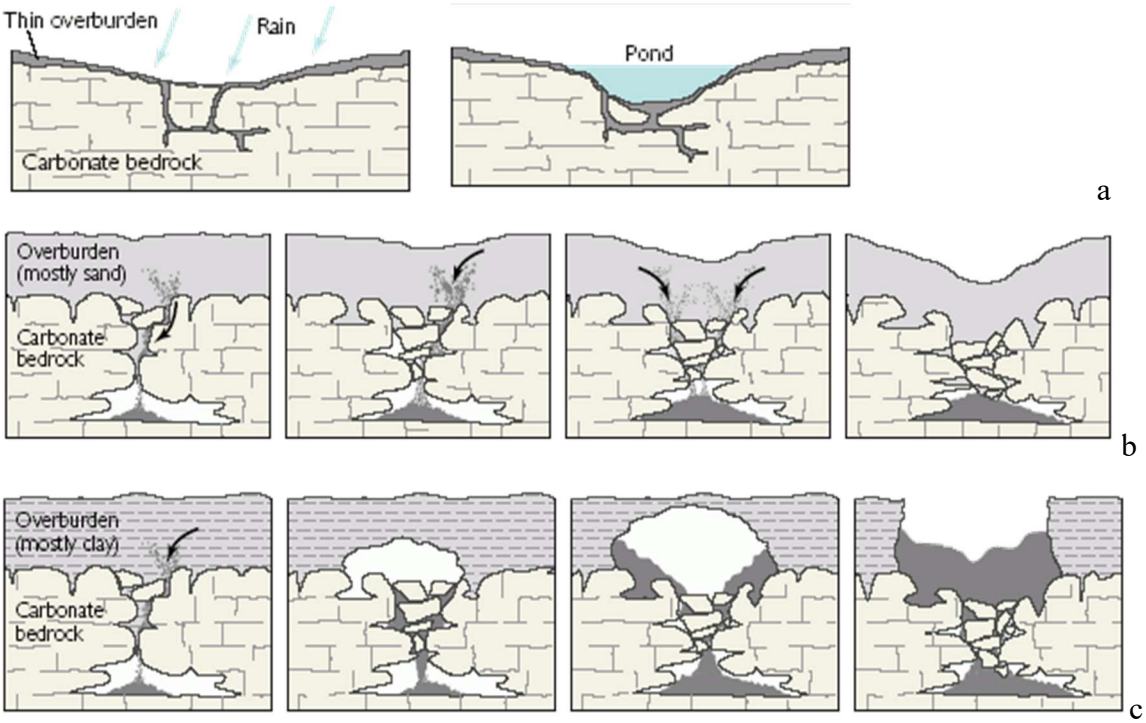

Figure 3.7. Three types of sinkholes: a. solution sinkhole; b. subsidence sinkhole; c. collapse sinkhole (USGS, 2018).

4. GEOPHYSICAL SURVEY

The geophysical surveys including ERT, MASW and SP surveys, all surveys include interpretation parts.

4.1. ELECTRICAL RESISTIVITY TOMOGRAPHY (ERT)

Electrical resistivity tomography (ERT) is an effective nondestructive geophysical tool for underground exploration. Resistivity is a fundamental property of the material. ERT can distinguish materials by quantifying how strongly the material resists the electric current. The resistivity of common materials is listed below (Figure 4.1).

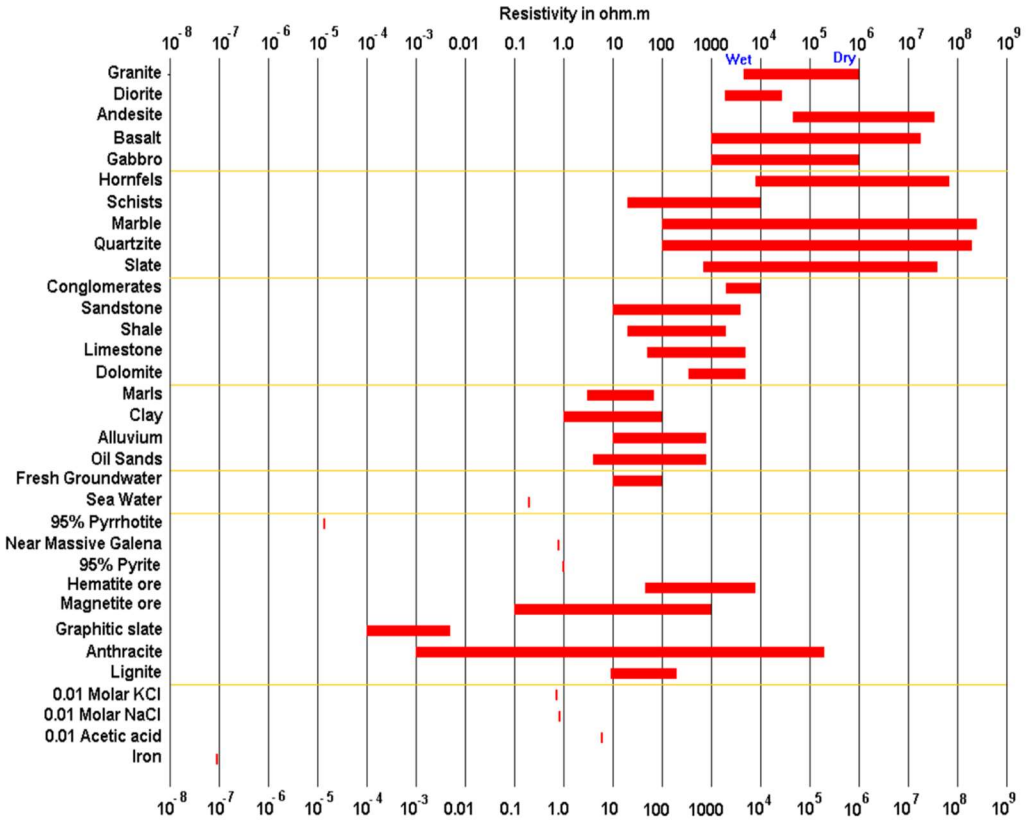

Figure 4.1.The resistivity range of common materials (Loke, 2004).

4.1.1. Philosophy. Electrical resistivity tomography survey is relatively straightforward. The equipment of ERT survey including SuperSting R8 (Figure 4.2-a), switch box (Figure 4.2-b), batteries (Figure 19-c), cable with electrode contact (Figure 4.2-d), and steel pins (Figure 4.3). The basic theory of ERT is using known AC current input into the ground using battery or generator and measuring the potential differences (ΔV). The resistance (***R***) of the subsurface can then be calculated using Ohm's law:

$$\Delta V = IR \tag{1}$$

where ***I*** is the current through the conductor in amperes, and ***R*** is the resistance of the conductor in ohms. The resistivity (***ρ***) is a nature of the material, it describes how strongly this material can resist the current flow. This property can be calculated using Equation (2) and (13):

$$\rho = k\frac{\Delta\emptyset}{I} \tag{2}$$

$$k = \frac{2\pi}{\left(\frac{1}{r_{C1P1}} - \frac{1}{r_{C2P1}} - \frac{1}{r_{C1P2}} + \frac{1}{r_{C2P2}}\right)}. \tag{3}$$

where ***k*** is a geometric factor function of electrode spacing, r_{C1P1} is the distance from current electrode C1 to potential electrode P1, r_{C2P1} is the distance from current electrode C2 to potential electrode P1, r_{C1P2} is the distance from current electrode C1 to potential electrode P2, and r_{C2P2} is the distance from current electrode C2 to potential electrode P2 (Figure 4.4).

4.1.2. Dipole-Dipole Array. Dipole-Dipole array is one of the arrays providing maximum resolution, is more sensitive of horizontal variation of the resistivity value and can be easily operated (Zhou, 2002). When using Supersting control unit, only four

electrodes are active at one time. In the dipole-dipole array, two electrodes serve as current electrodes, and two electrodes serve as voltmeter electrodes (Figure 4.5). The survey procedure of dipole-dipole array is just like a printer. As an example, the survey using dipole-dipole array starts with the spacing of *a* between C_1 C_2 and P_1 P_2. For a shallower subsurface, the space between C_2 and P_1 is 1a. A potential data will be measured and marked in the the middle of the space and then four electrodes will shift to the right. The second sequence of measurement is the *2a* space between C_2 and P_1 (Figure 4.6). For subsequent measurements, the n spacing factor is usually increased to a maximum value of about 6 (Loke, 2004).

Figure 4.2. Equipments of ERT survey: a. supersting control unit; b. switch box; c. battery; d. survey cable.

Figure 4.3. The setup of an ERT system.

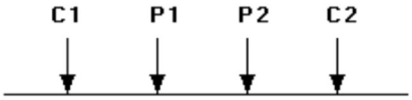

Figure 4.4. A conventional array with four electrodes to measure the subsurface resistivity (Loke 2004).

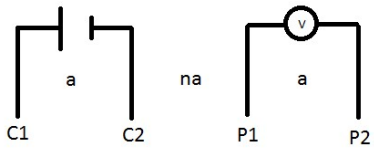

Figure 4.5. The principle of the dipole-dipole array in ERT survey.

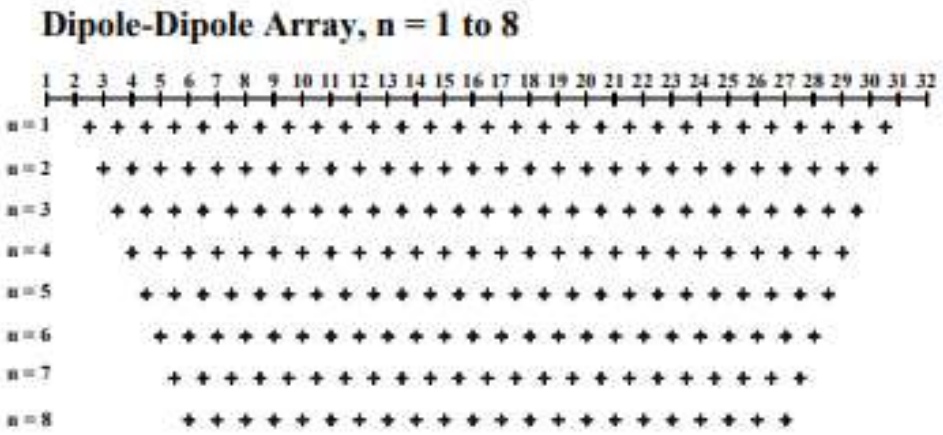

Figure 4.6. Pseudo-depth distribution of data points for dipole-dipole array configurations (Batayneh, 2005).

4.1.3. ERT Data Interpretation. A total of 12 ERT profiles with seven NNE/SSW-oriented ERT profiles (named1-7) and five W/E oriented ERT profiles (named A-E) were set for interpretation. These data will be plotted separately in Appendix A.

In the study area, most clayey soil characterized by resistivity values that less than 45 ohm-m. Weathered or fractured limestone with a significant amount of clay infill was characterized by resistivity values less than 90 ohm-m. Moist weathered or fractured limestone was characterized by resistivity values between 90 ohm-m and 250 ohm-m. Intact/drier limestone was characterized by resistivity values greater than 250 ohm-m. The resistivity greater than 1000 ohm-M may adjust the grout which injected by Strata Services, Inc. An example of the ERT profile is in Figure 4.9.

Typically, the soil and weathered rock which has better porosity will contain more moisture material and have less resistivity. The interpreted top-of-rock was shown in a zone with low elevation on the northeast side of the lake, which was situated at the place

marked by Shannon & Wilson, Inc. as a sinkhole that developed in 2004 (Figure 2.1 and 4.7).

Most of the rocks below elevation 600 ft. is good quality rocks with resistivity much greater than 250 ohm-m. The rock below elevation 600 ft. is classified as either moist weathered/fractured limestone or intact drier limestone. The resistivity of rock at elevation above elevation 600 ft. decreases significantly. Rock above elevation 600 ft. is classified as intensely moist weathered/fractured limestone with clay infill. The rock at elevation between 600 ft. and 630 ft. shown lower resistivity than the rock at elevation above 630 ft. and below 600 ft. This may represent the lateral conduit for laterally flowing groundwater or represent the development of small sinkholes that allow lake water flow vertically through the overlying rock (rock above 630 ft.) into the interpreted area.

In Figure 4.10 and 4.11, solution-widened joints with resistivity lower than 90 ohm-m were identified. These low resistivity zones extend to elevations below 600 ft. at ERT profile 1 station 400 (Figure 4.10 and Figure A1), ERT profile 7 station 440, 740, and 900 (Figure 4.10 and Figure A7) may represent a rock zone with significant porosity, permeability anomalous and with significant amount of moist clay infill which could represent the past or current pathway for vertically flowing groundwater. Two prominent low resistivity zones were found in ERT profile A station 140 and 400 (Figure 4.11 and Figure A8). Because ERT profile A is the nearest W/E oriented ERT profiles to the south of the dam, these two low resistivity zones could represent seepage zones that allow horizontally flow of groundwater through North Dam.

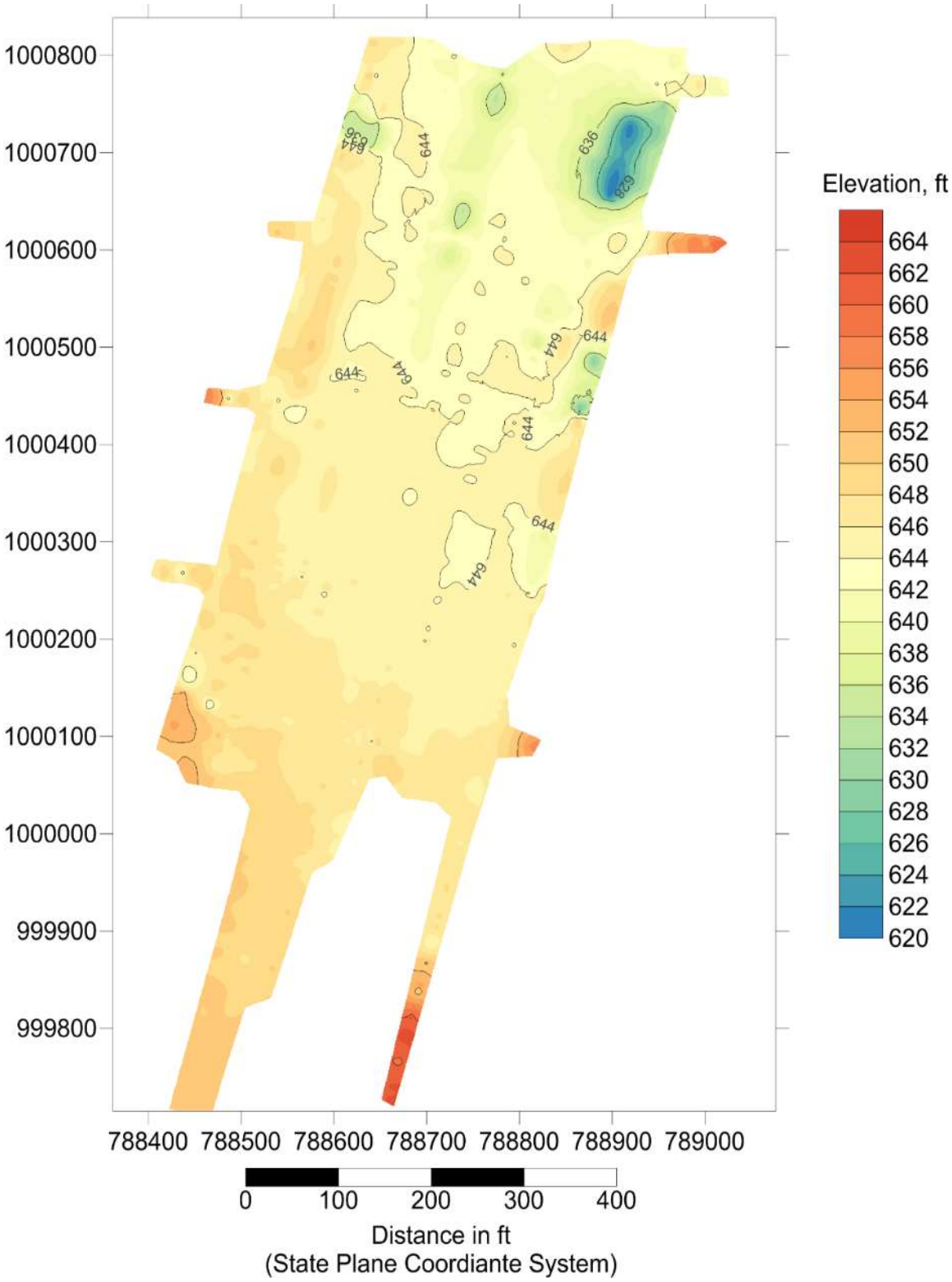

Figure 4.7. The top-of-rock elevations are consistent with the Shannon & Wilson, Inc. report and the top-of-rock as identified on the interpreted MASW shear-wave velocity profiles.

4.2. MULTI-CHANNEL ANALYSES OF SURFACE WAVES (MASW)

Multi-channel analyses of surface waves (MASW) were used with Rayleigh waves to investigate subsurface stratum distribution. The mechanism of this method based on the disparity of materials in shear wave velocity. The classification of soil and rock base on the National Earthquake Hazards Reduction Program (NEHRP) guidelines. NEHRP site classification definitions are based on the calculated shear-wave velocity and is listed in Figure 4.8.

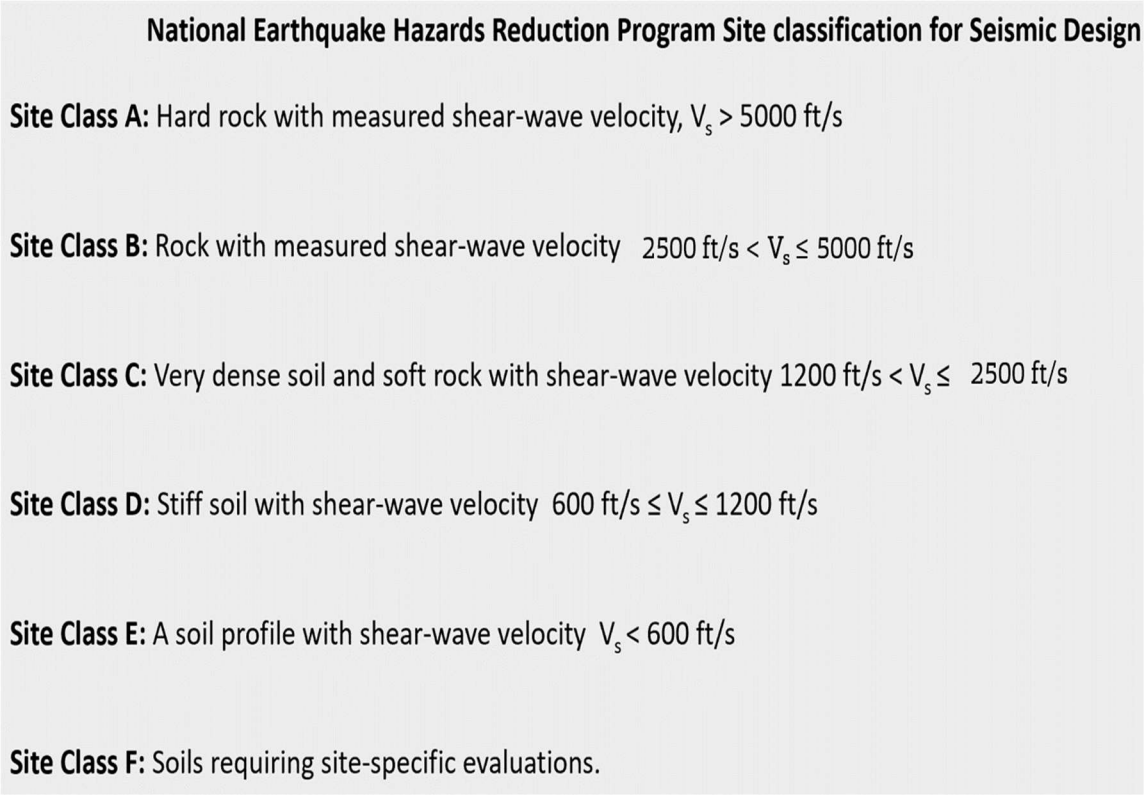

Figure 4.8. The classification of soil and rock based on NEHRP guidelines.

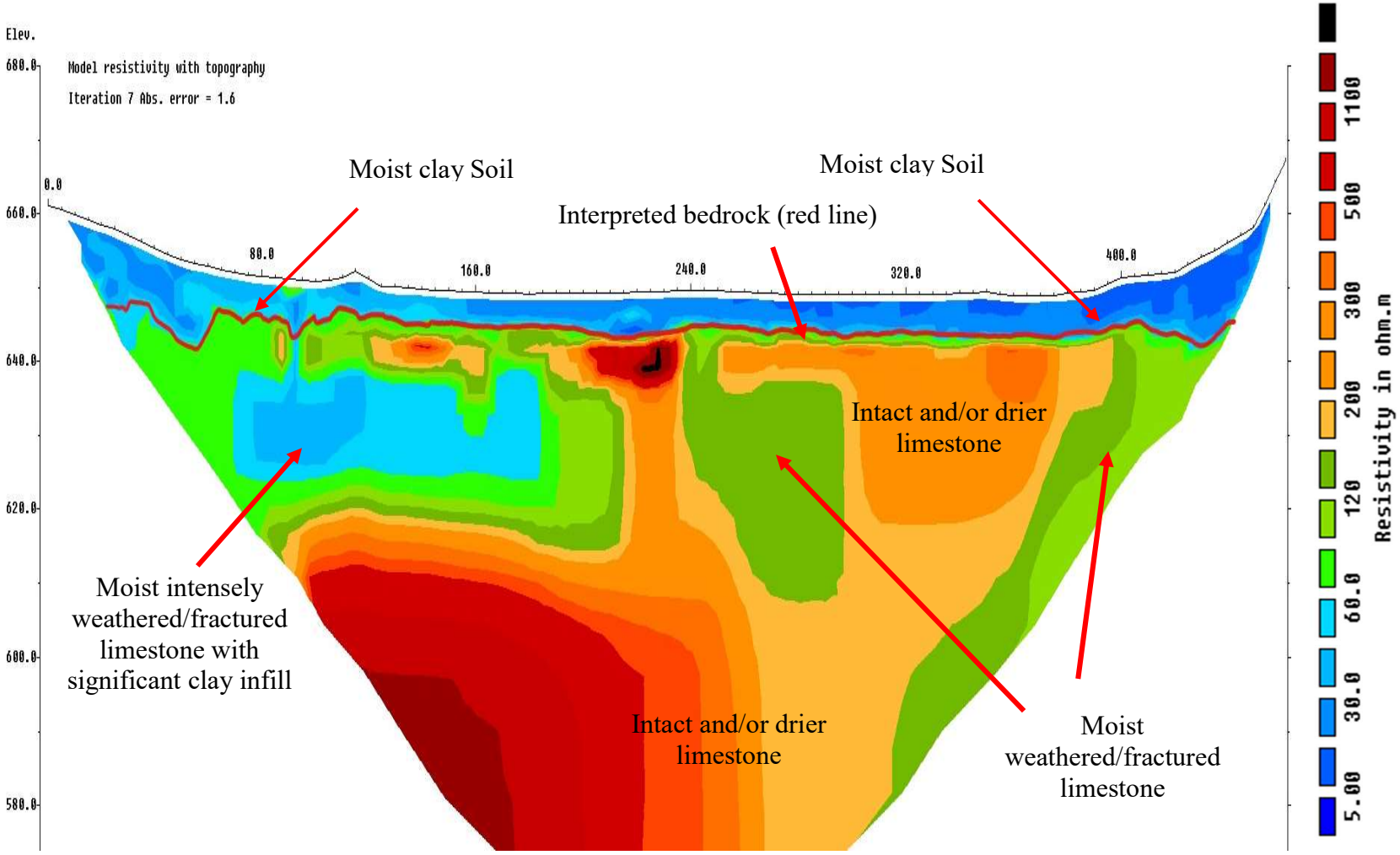

Figure 4.9. Example ERT profile (ERT profile D). The interpreted top of rock (red line) correlates well with the 45 ohm-m contour interval.

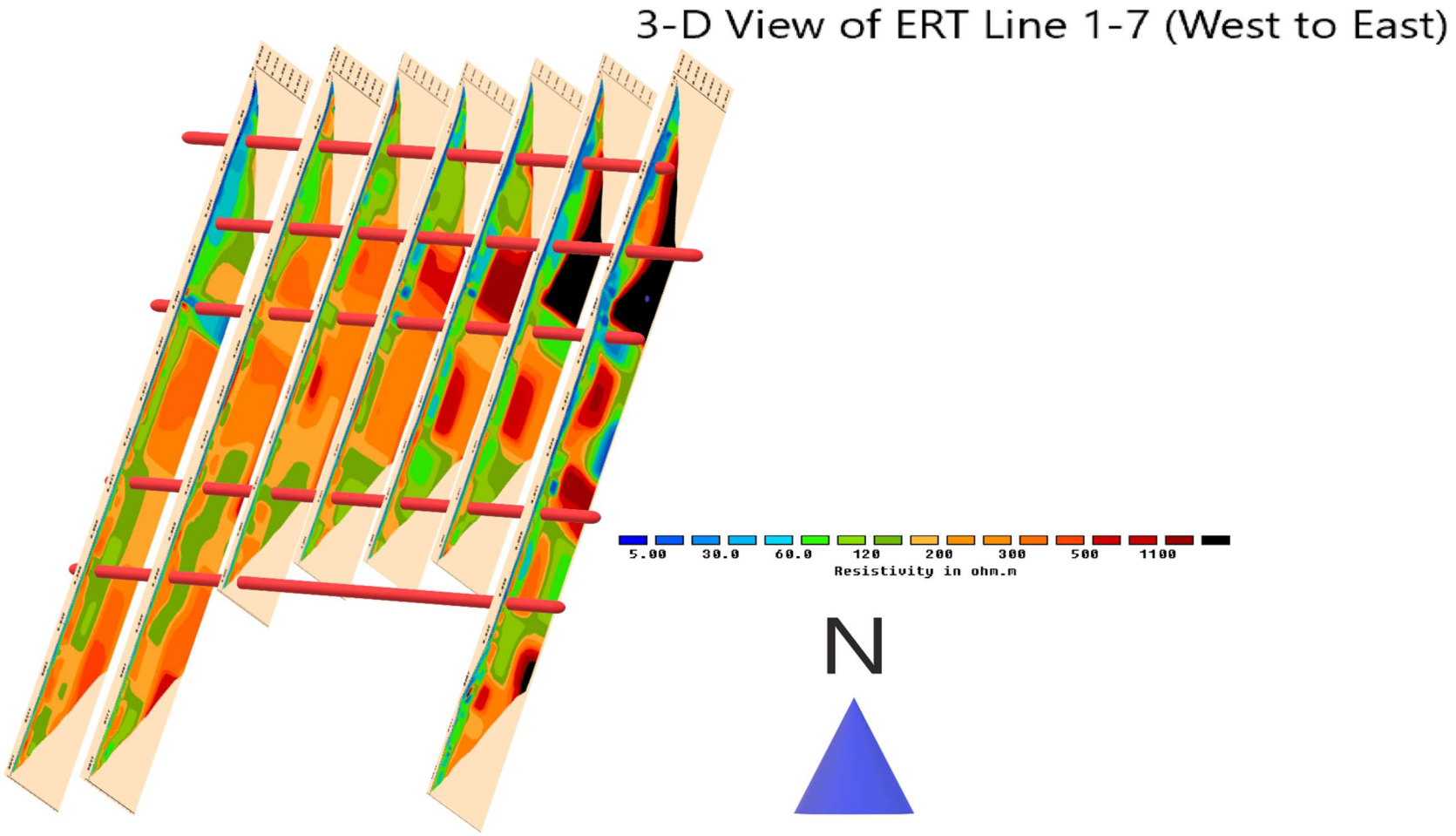

Figure 4.10. 3-D NNE/SSW oriented ERT profiles 1-7 (Figure 2.1). Red lines were used to connect the solution-widened joint features from each profile. Distances and elevations are in ft., detailed interpretations of ERT profiles 1-7 are presented in Appendix A.

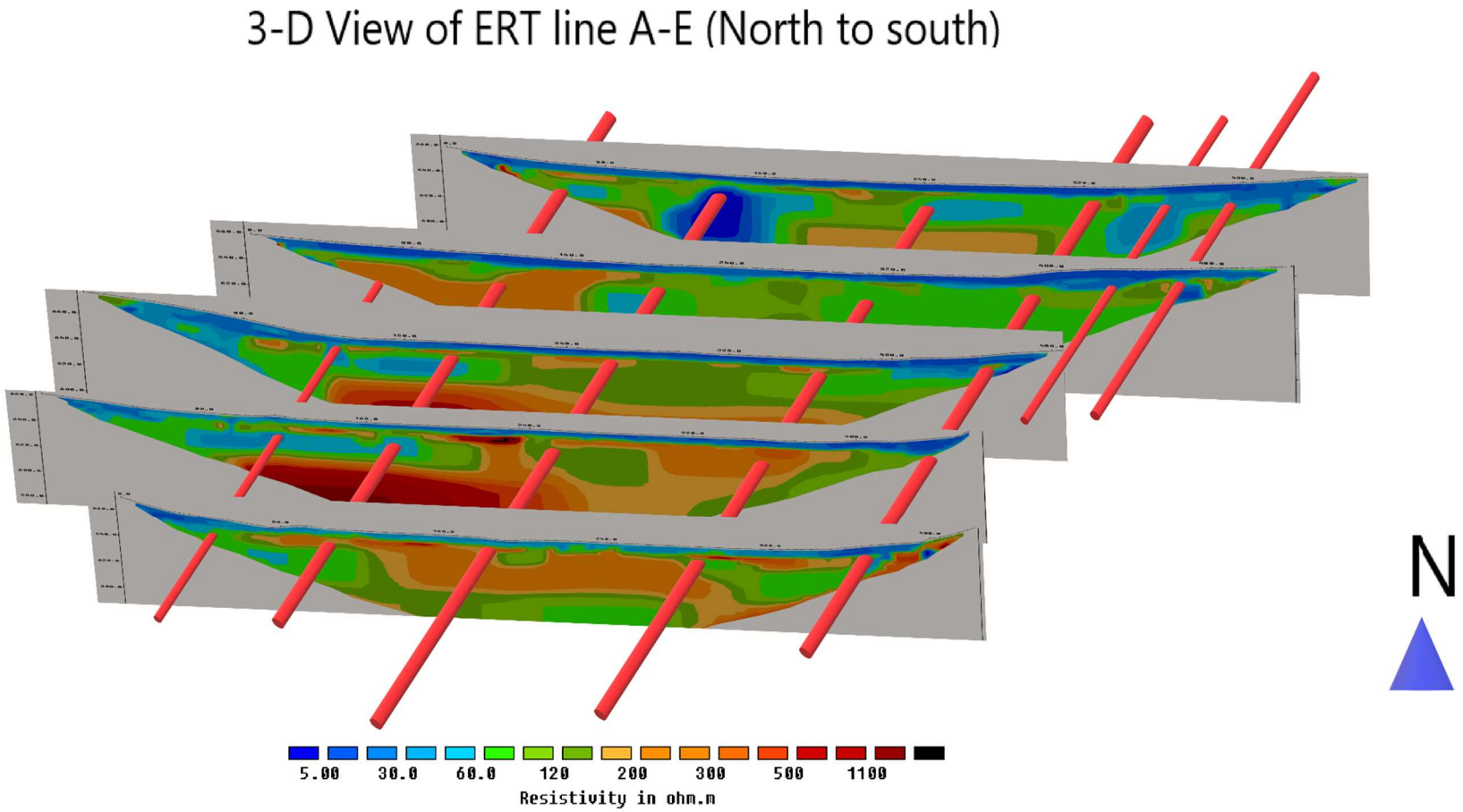

Figure 4.11. 3-D view of W/E oriented ERT profiles A-E (Figure 2.1). Red lines were used to connect solution-widened joint features from each profile. Distances and elevations are in ft. More detailed interpretations of ERT profiles A-E are presented in Appendix A.

4.2.1. Philosophy. MASW survey equipment in this study includes 4.5 Hz geophones (Figure 4.12-a), battery (Figure 4.12-b), a 20-pound sledge hammer (Figure 4.12-c), and a 24-channel engineering seismograph (Figure 4.12-d). The basic theory of MASW uses a sledge hammer to generate Rayleigh waves; the wave signal was collected by geophone for data processing. After the data processing, surface waves can be divided into the higher mode and the fundamental mode due to dispersive properties. Dispersion is the phenomenon in which phase and group velocities of a surface wave depend on frequency (MacIntyre, nd). Higher frequencies involve particle motion at shallower depths and lower velocity; lower frequencies involve particle motions at greater depths and higher velocity. In a layered media, the frequency of a surface wave is related to the elastic and physical properties of the material (Lee et al., 2002). According to Anderson and Thitimakorn's report, in a homogeneous (non-dispersive) medium, Rayleigh wave phase velocities are constant and can be determined using the following Equation (4):

$$V_R^6 - 8\beta^2 V_R^4 + (24 - 16\beta^2/\alpha^2)\beta^4 V_R^2 + 16(\beta^2/\alpha^2 - 1)\beta^6 = 0 \quad (4)$$

where V_R is the Rayleigh wave velocity within the uniform medium, β is the shear-wave velocity within the uniform medium (also denoted Vs), and α is the compressional wave velocity within the uniform medium (also denoted Vp).

Compared with compressional wave (P-wave), a Rayleigh wave is more sensitive to shear wave (S-wave). To convert Equation 4 to the relation between V_R and β, the relation between α and β should first be resolved. The Scalar wave equation explains the relation between compressed wave, shear wave, density, bulk modulus, and shear modulus:

$$\alpha = \sqrt{(\lambda + 2\mu/\rho)} \quad (5)$$

$$\boldsymbol{\beta = \sqrt{(\mu/\rho)}} \quad (6)$$

where $\boldsymbol{\alpha}$ is the compressional wave velocity, $\boldsymbol{\beta}$ is the shear-wave velocity, $\boldsymbol{\rho}$ is the density of the material, $\boldsymbol{\lambda}$ is bulk modulus and $\boldsymbol{\mu}$ is shear modulus. Hooke's law summarized the relation between bulk modulus, shear modulus and Poisson's ratio:

$$\boldsymbol{\sigma = \lambda/2(\lambda + \mu)} \quad (7)$$

where $\boldsymbol{\sigma}$ is Poisson's ratio. By combining Equation 5, 6 and 7 we can get the relation of $\boldsymbol{\alpha}$ and $\boldsymbol{\beta}$ as:

$$\boldsymbol{\frac{\beta}{\alpha} = \sqrt{(0.5 - \sigma)/(1 - \sigma)}} \quad (8)$$

the values of Poisson's ratio for many materials are close to the initial recommendation of 1/4 by Poisson by Wertheim (Gercek, 2007), so the Equation 8 should equal to 1/3. Using this relation of the shear wave and compressional wave in equation 4 will result in Equation (9):

$$\boldsymbol{V_R}=0.919\ \boldsymbol{\beta} \quad (9)$$

which shows that V_R is directly related with $\boldsymbol{\beta}$. When V_R varies with depth, we can determine how $\boldsymbol{\beta}$ varies with depth.

4.2.2. MASW Data Processing. Data processing was performed using Surfseis which developed by Kansas Geologic Survey (KGS). The fundamental processing is to image all types of waves (including body and surface waves) from short gather (Figure 4.13) to dispersion-curve (Figure 4.14) using the wavefield-transformation method (Park et al., 1998; Luo et al., 2008). This converting process can generate dispersion patterns that can be more easily recognized by visually sorting out the possible fundamental mode to convert data to 1-D shear-wave velocity inversion (Figure 4.15).

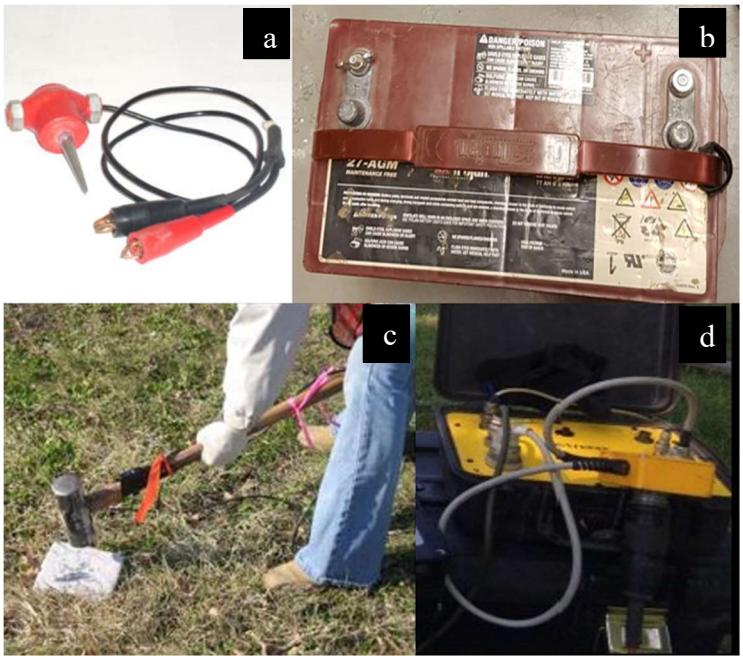

Figure 4.12. MASW equipment overview. a. 4.5Hz geophone. b. 12V battery. c. 20 lb sledge hammer. d. 24-channel engineering seismograph.

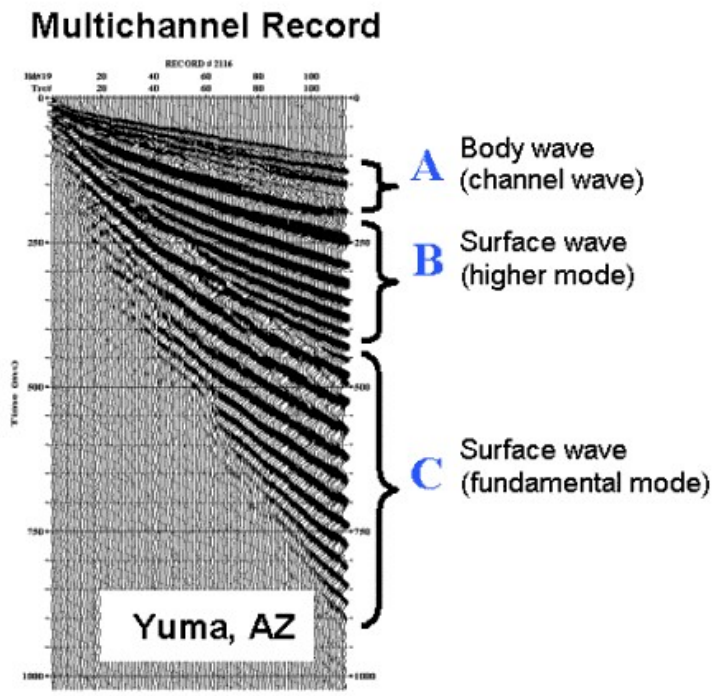

Figure 4.13. Shot gather sample (Kansas Geological Survey Academic and Science (KGS, 2014).

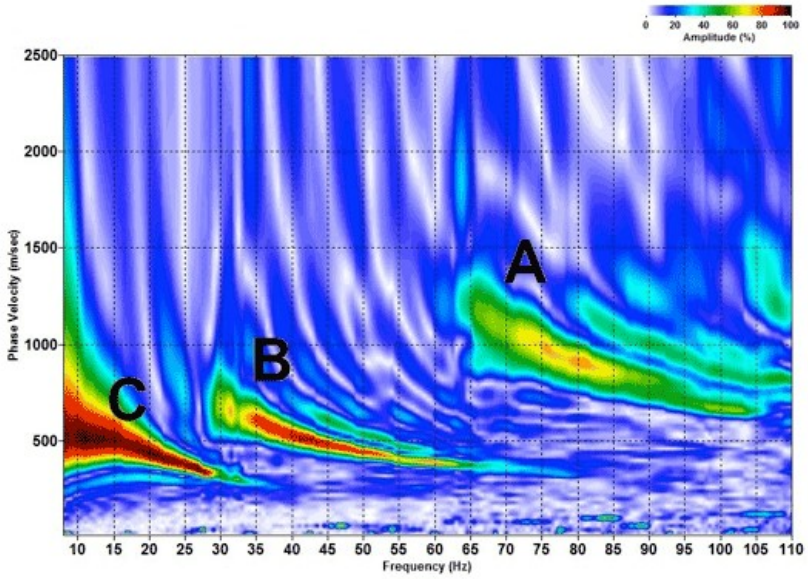

Figure 4.14. Converted dispersion curve of shot gather in the figure. A represent body wave, B represent higher mode, C represent fundamental mode (KGS, 2014).

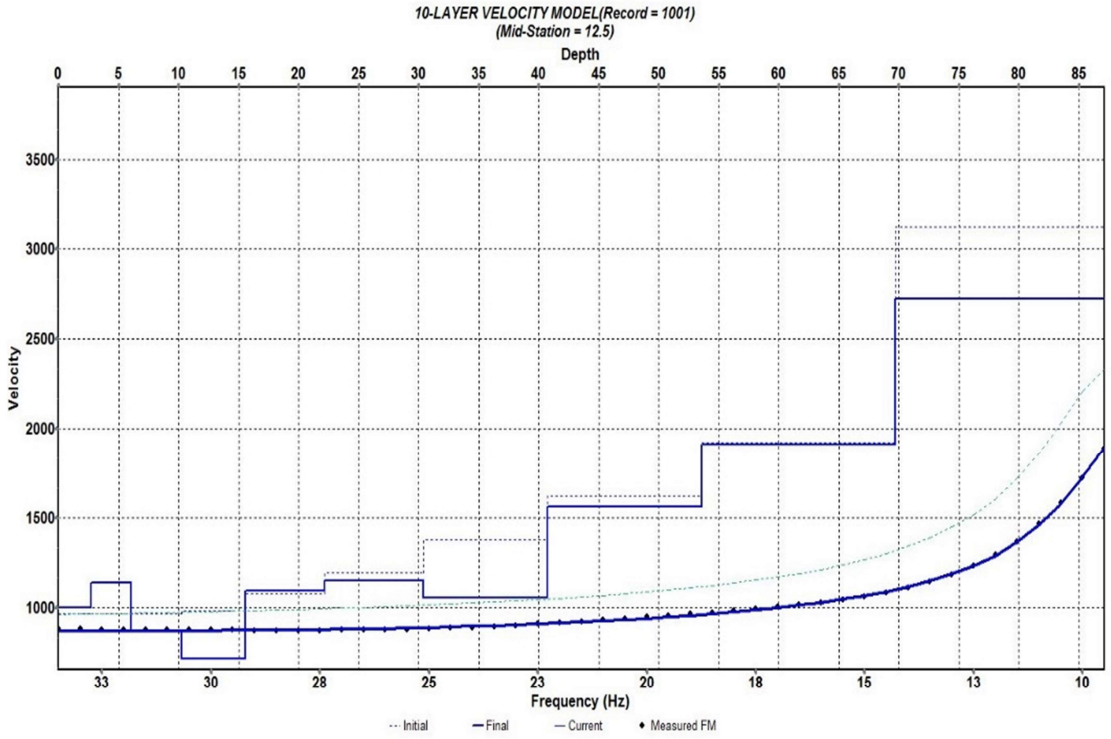

Figure 4.15. Sample 1-D shear-wave velocity profile generated using Surfseis.

4.2.3. MASW Data Interpretation. Five MASW sets (1-D shear-wave velocity profile) are presented in Appendix B (Figure B1-B5). All MASW datasets are correlate well with ERT profiles. According to the data interpretation, the upper layer of soil is characterized by shear-wave velocities less than 1000 ft/s. The top of the weathered rock characterized by the shear-wave velocities greater than 1000 ft/s. The top of the intact/dry rock picked as the shear-wave velocity greater than 2500 ft/s (Figure 4.16).

1-D shear wave profile generated by MASW data estimates of depth to the top of weathered rock and intact rock correlate well with ERT profile. Location of MASW profile 1, 2 and 5 are close to ERT profile 7 at station 60, station 190, and station 800 (Figure 4.17). Location of MASW profile 3 is close to ERT profile 2 at station 200 (Figure 4.18). Location of MASW profile 4 is close to ERT profile 5 at station 670 (Figure 4.19).

Slight discrepancies between the MASW and ERT interpretations occur is acceptable, because using the MASW method to interpret the top of weathered rock based on acoustic velocity and using ERT method to interpret the top of weathered rock based on resistivity. Hence, error smaller than 5 ft. between ERT and MASW profile will not be counted.

Both interpretations of MASW and ERT data support the concept that rock at elevations below 600 ft. is significantly less weathered than the rock at elevation above 600 ft. Some places below beds of weathered rock show that lower shear-wave velocities will probably be the zone that have highly weathered/fractured rock with moisture clay infill, which could be the lake water seepage path. This observation is consistent with the interpretation of the ERT data.

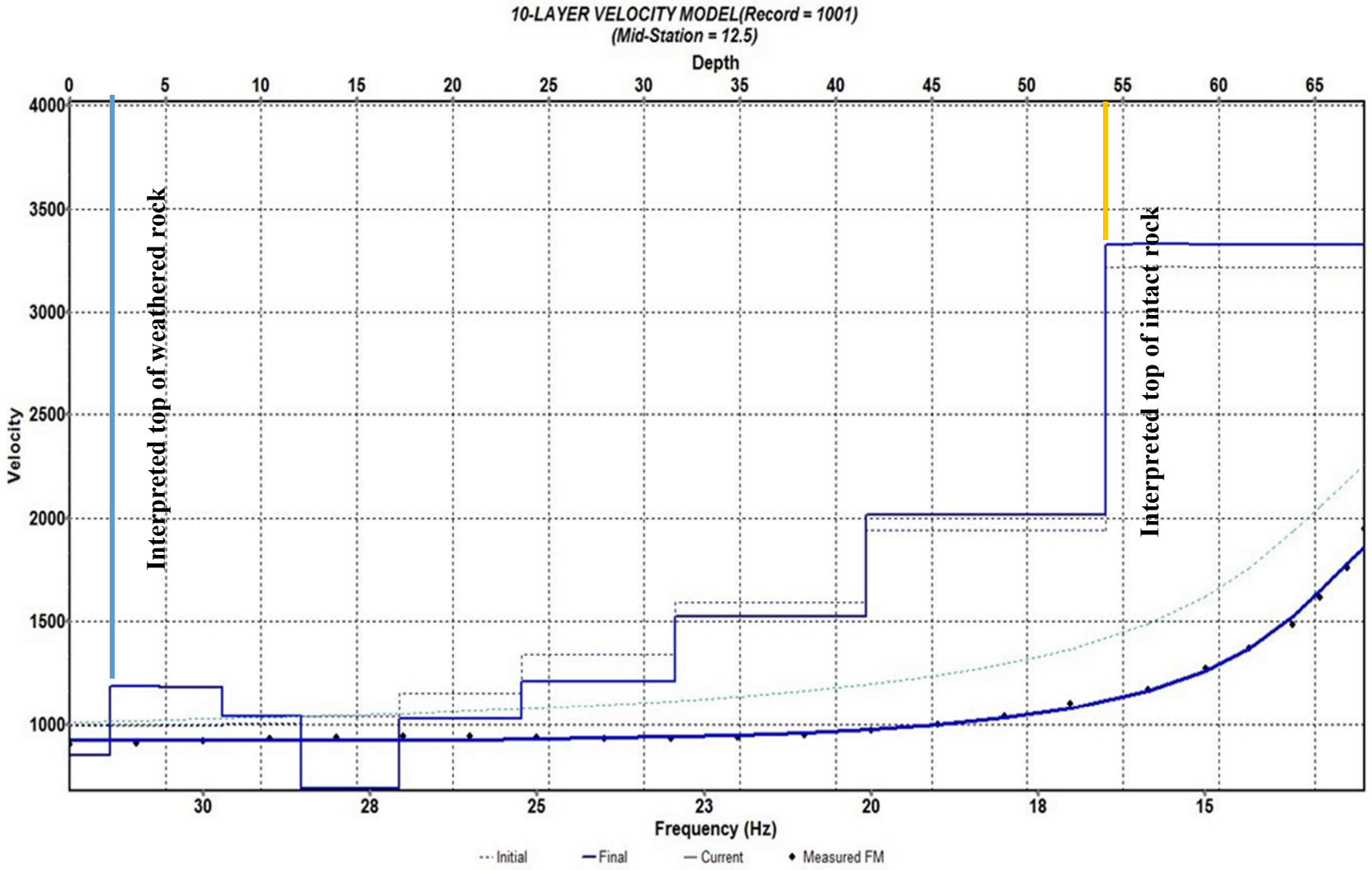

Figure 4.16. Sample interpretation 1-D shear-wave velocity profile MASW 1.

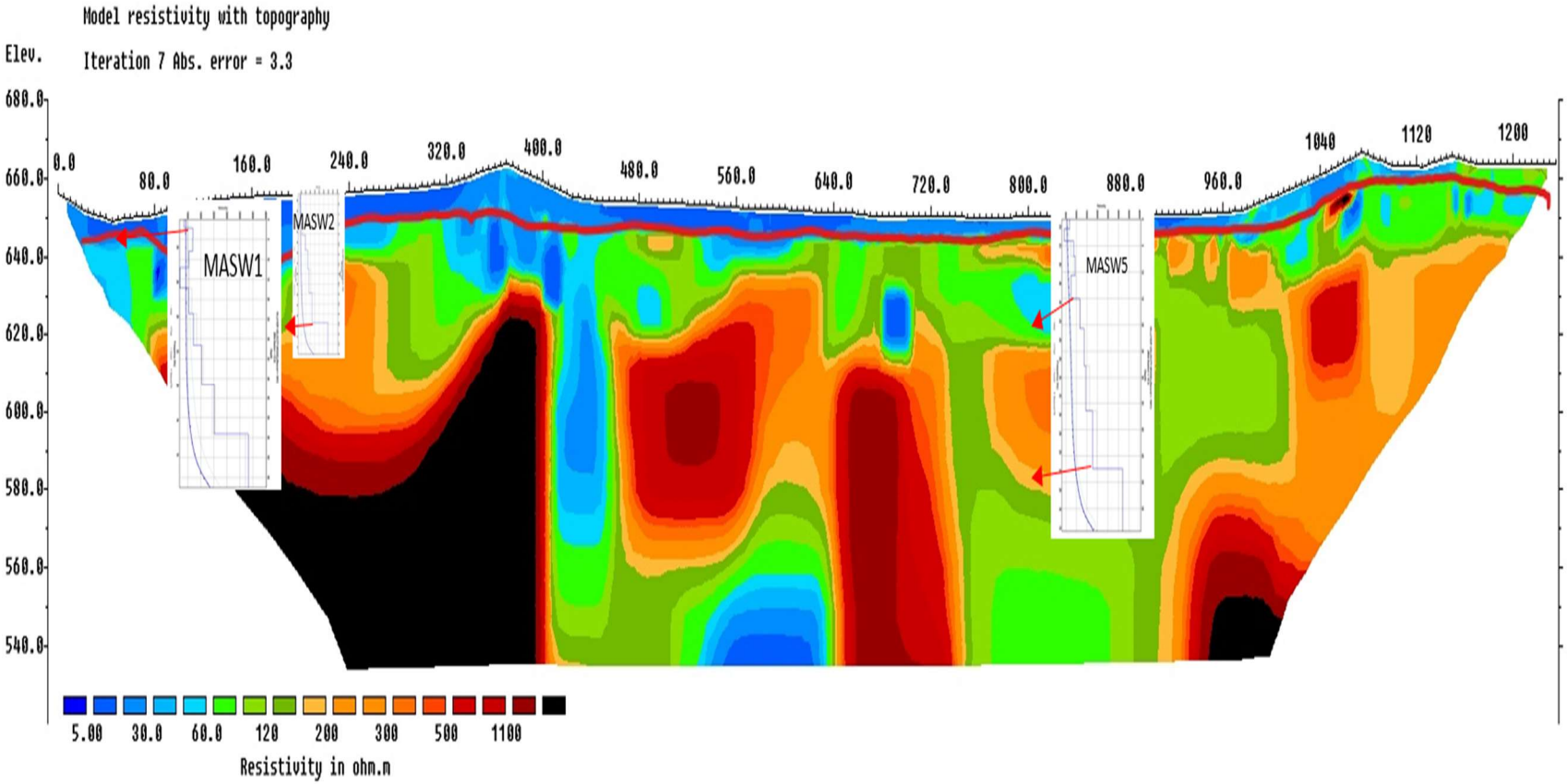

Figure 4.17. MASW 1-D shear-wave velocity profile 1,2,5 correlate well with ERT profile 7 at station 60, 190, and 800.

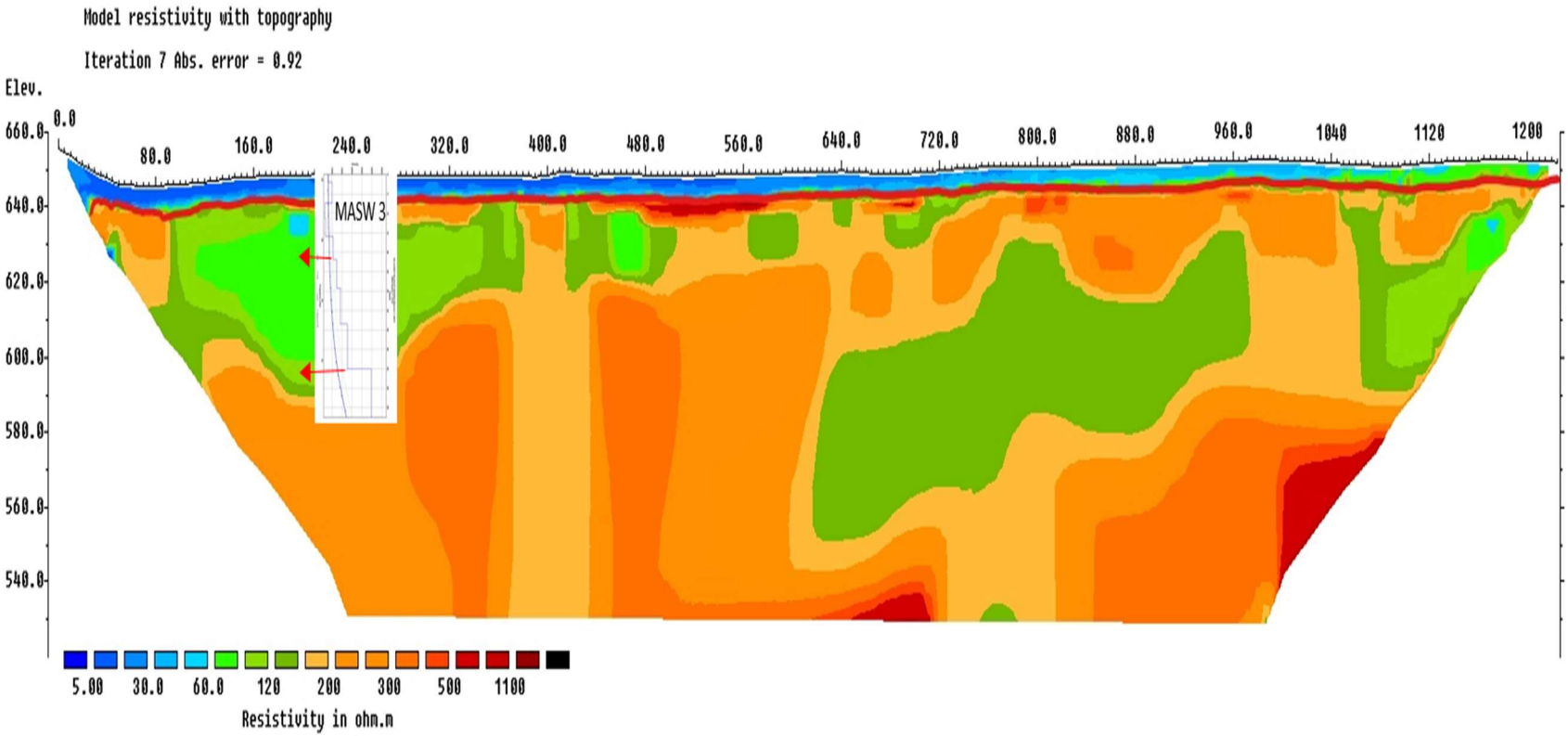

Figure 4.18. MASW 1-D shear-wave velocity profile 3 correlate well with ERT profile 2 at station 200.

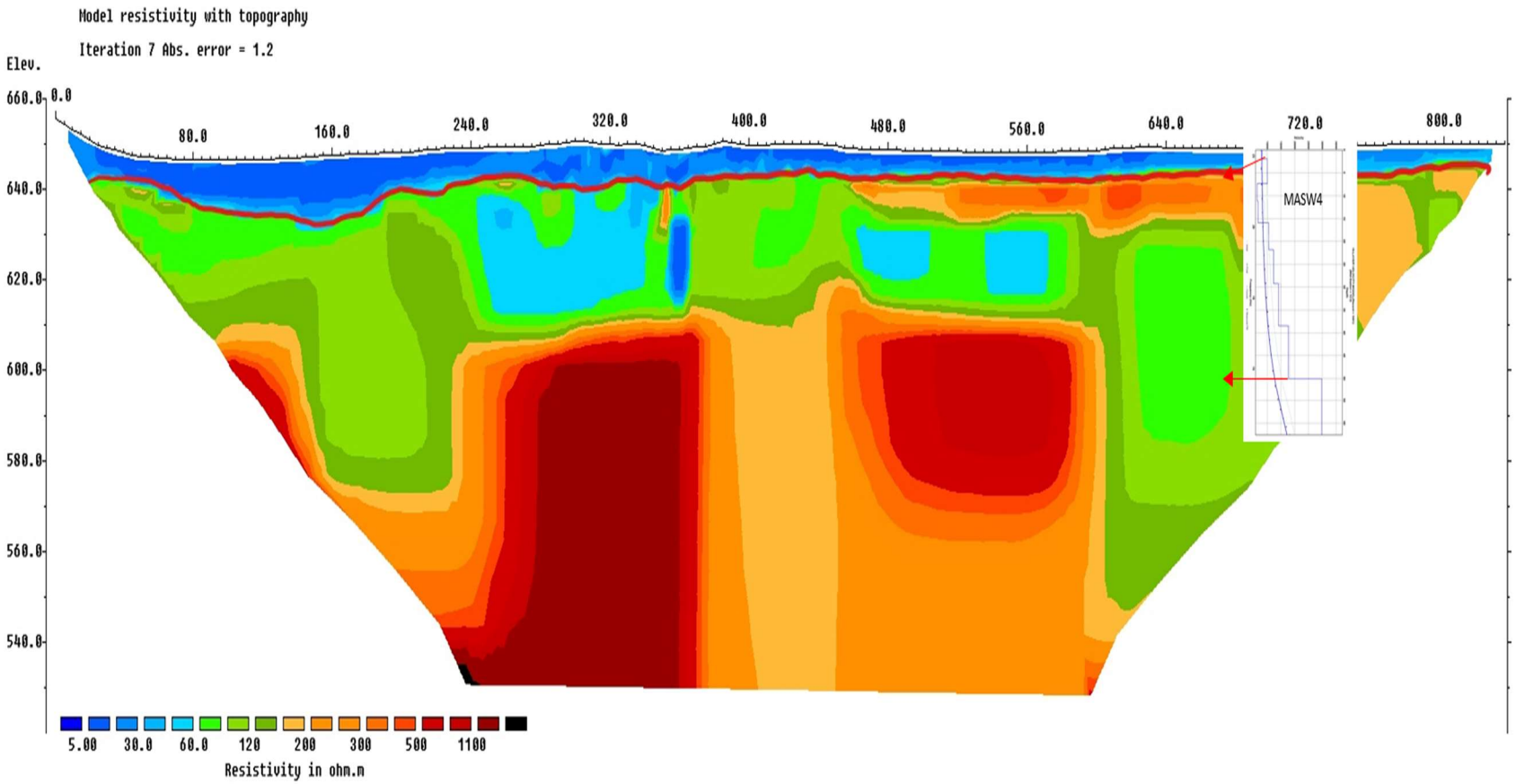

Figure 4.19. MASW 1-D shear-wave velocity profile 4 correlate well with ERT profile 5 at station 670.

4.3. SPONTANEOUS POTENTIAL (SP)

Spontaneous potential tool also called the self-potential tool, is used to map naturally occurring electric potential difference.

4.3.1. Philosophy. The spontaneous potential tool used in this study contains base electrode, lead electrode (Figure 4.20–a), cable (Figure 4.20-b), and Supersting control unit (Figure 4.20–c). Natural potential occurs under many different conditions, like dissimilar materials, flow of fluids, and varying concentration of electrolytic solutions. When detecting ground using the SP tool, those bodies act as batteries. The SP tool acts like a voltmeter that can detect natural current. Natural current flow in the subsurface is electrolytic. When springs, underground streams, or seepage through earth fill dams, SP anomalies show negative.

SP can be divided into two types: streaming potential and electrochemical potential. Streaming potential generated from the flow of water over naturally charged soil (or solids). From Delgado's research (2005), the value of streaming current observed in a capillary is usually related to the zeta potential through Equation (10):

$$I_{str} = -\frac{\epsilon_{\tau s}\epsilon_0 \alpha^2 \pi}{\eta}\frac{\Delta P}{L}\zeta \tag{10}$$

From the Helmholtz-Smoluchowski equation, the streaming potential across the flow system is:

$$U_{str} = \frac{\epsilon_{\tau s}\epsilon_0 \zeta}{\eta K_L}\Delta P \tag{11}$$

where I_{str} is streaming current under short-circuit conditions; U_{str} is streaming potential at zero net current conditions; $\epsilon_{\tau s}$ is relative permittivity of the liquid; ϵ_0 is electrical permittivity of vacuum; η is dynamic viscosity of the liquid; ζ is zeta potential; ΔP is

pressure difference; L is capillary length; and K_L is specific conductivity of the bulk liquid. From Renner's book (2007), the electrochemical potential was defined as the partial molar Gibbs energy of the substance at the specified electric potential, where the substance is in a specific phase, which can be described as:

$$\bar{\mu}_i = \mu_i + z_i F \Phi \quad (12)$$

where $\bar{\mu}_i$ is the electrochemical potential of species; μ_i is the chemical potential of the species; z_i is the valency of the ion I; F is the Faraday constant; and Φ is the local electrostatic potential.

4.3.2. SP Data Interpretation. A total of 690 SP points was tested in the field; the result is plotted as contour map (Figure 4.21). Three anomalous area were identified and are labeled as SP1, SP2, and SP3. SP1 was situated near the eastern shoreline. SP2 was situated in the north part of ERT 1, 2 and 3. Only one data point in SP3 was shown negative, and no neighboring points had similar data. This abnormal area might create by mistake during the survey. The interpretation of SP data is consistent with the interpretation of the ERT profiles. SP anomalies are observed in areas where ERT anomalies are present.

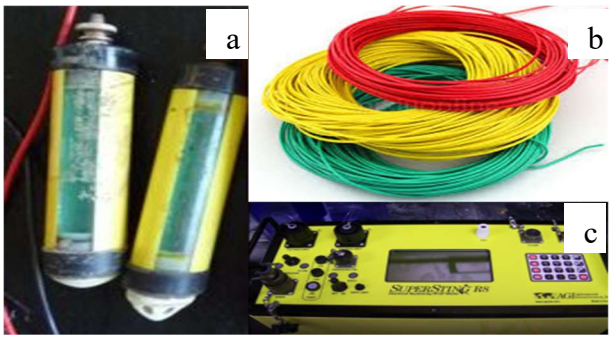

Figure 4.20. SP equipment in this study: a. base and lead electrode; b. electric cable; c. Supersting.

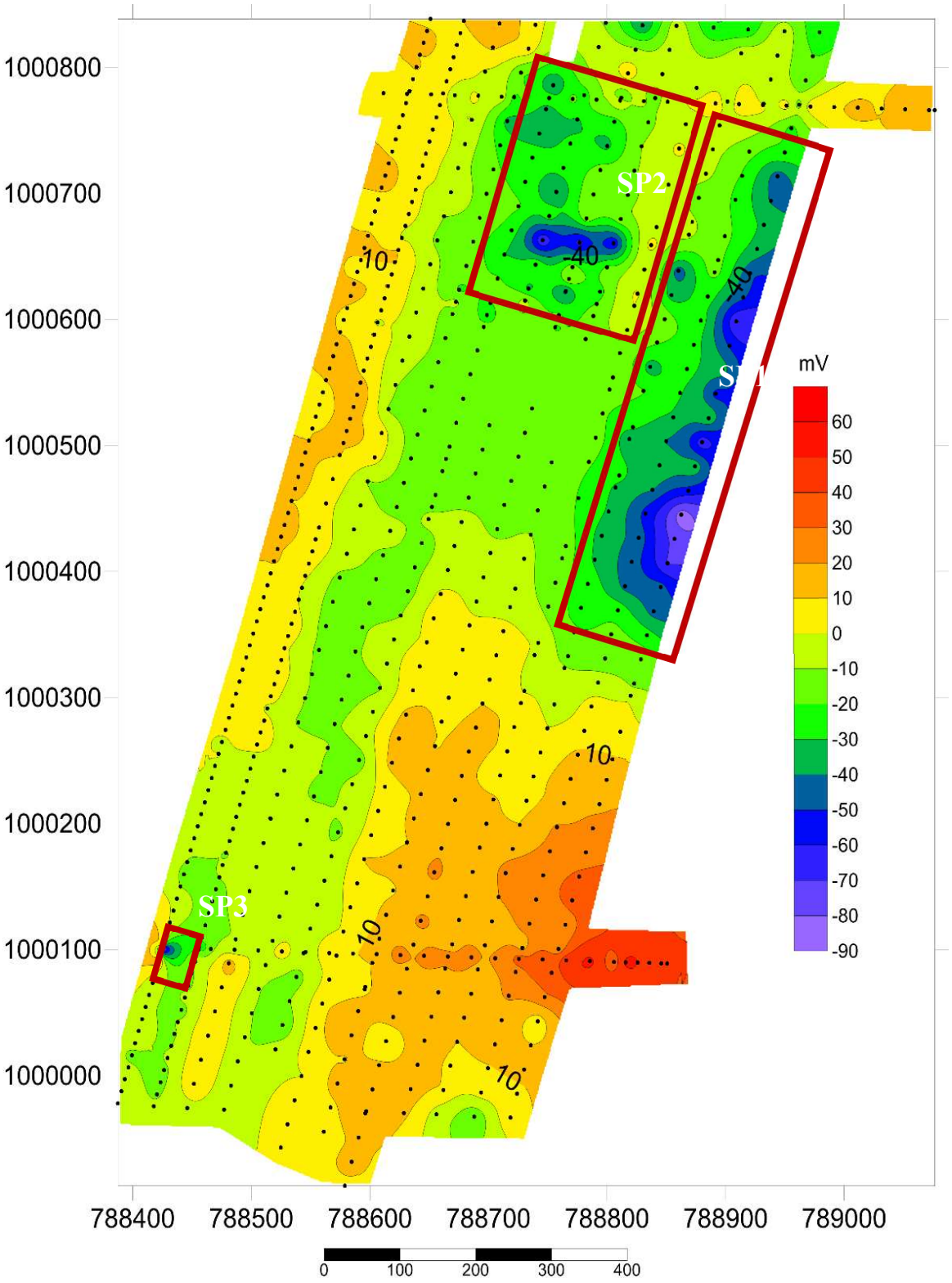

Figure 4.21. Contoured plot of the SP data acquired in the field, SP1 and SP2 were interpreted as seeping vertically into the subsurface. The anomalous areas were marked using red rectangles.

5. CONCLUSIONS

The objectives of this study were: 1) Mapping depth to the top of the rock of the Lake Chesterfield; 2) identify karst features, like sinkholes and joints; 3) finding potential seepage area; and 4) map shear velocity of soil and rock. A total of 12 ERT profiles, 5 MASW sites, and 690 SP points were processed and interpreted.

5.1. INTERPRETED TOP OF BEDROCK

Bedrock of study site (Lake Chesterfield) that interpreted by ERT and MASW data are situated at average 9 to 10 ft. below the surface. This result is consisting with the test pit result generated by Geotechnology, Inc. in the 'Subsurface Exploration – Dams and Lakes' report.

5.2. ROCK QUALITY

For rock quality, most bedrock above elevation 600 ft. in Lake Chesterfield is poor quality and identified as weathered/fractured limestone with low resistivity and low shear-wave velocity, which could serve as conduit for laterally flowing groundwater. From the ERT profiles, some low resistivity and low shear-wave velocity zones have similar features and can be driectly connected, which could characterized as solution-widened joints.

5.3. SOLUTION-WIDENED JOINTS

According to the interpretation of ERT profiles, the study area appears to be dissected by NNE/SSW and W/E trending solution-widened joints**.** These joints may serve as conduits for vertically percolating or flowing of lake water. In places, the

fractures appear to extend to elevations below 600 feet (as interpreted on the ERT profile) and could extend to elevations significantly below 600 feet.

5.4. SEEPAGE PATHWAYS

According to the report generated by Geotechnology, Inc., Lake Chesterfield dam was built at elevation 645 ft. with 5 ft. extended cutoff trench (Figure 5.1). Base on the survey in this study, poor-quality rock zones could extend to elevation 600 ft. That means the dam was built on the poor-quality rock that could easily develop karst feature. After filling of water, the pressure will increase and create the seepage pipe beneath the dam and cause the leakage issue.

5.5. POTENTIAL SEEPAGE PATH THROUGH NORTH DAM

According to the interpretation of ERT data. Area between station 100 and 170, in addition, area between station 330 and 370 in ERT profile A characterized by low resistivity zone. If the resistivity anomaly was not caused by the metal drain, these areas could be highly weathered rock with significantly clay infill and served as potential seepage pathway through the North Dam.

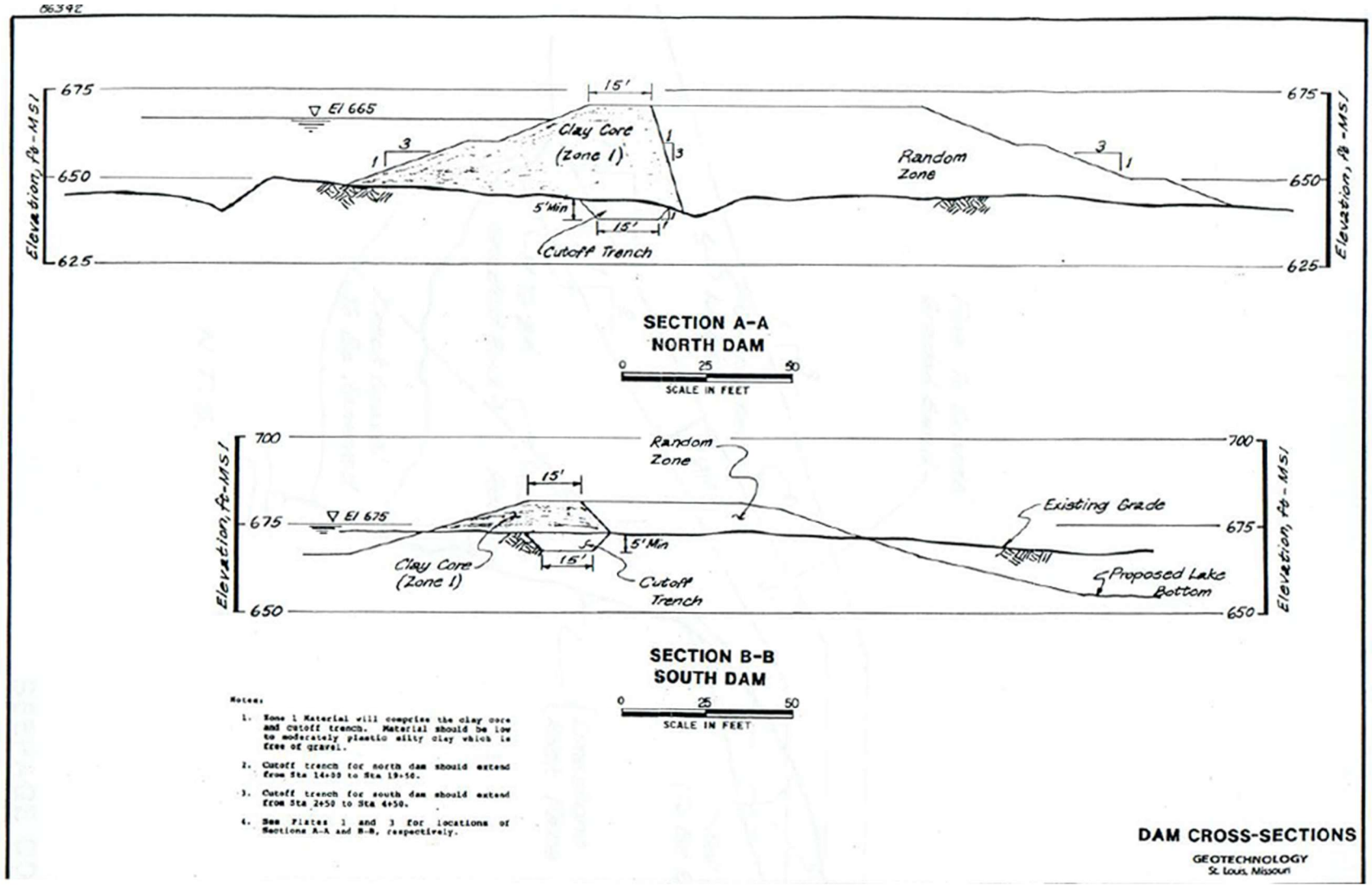

Figure 5.1. Dam cross section generated by Geotechnology, Inc. from 'Subsurface Exploration – Dams and Lakes Report'.

6. RECOMMENDATIONS

Based on the interpretation of geophysical data, two suggestions were made to minimize leakage, one suggestion is grouting; the other suggestion is emplacement of liner.

For grouting method, drilling test boreholes at location between station 100 and 170, in addition, location between station 330 and 370 in ERT profile A is recommended. If grouting determined to be a viable option, acquiring additional geophysical data across the grouting area is recommended.

For emplacement of new liner, acquiring borehole data in areas identified on the geophysical traverses as anomalous (poor quality, low resistivity rock) is recommended. The liner should be designed on the potential for the erosion of the liner along the shorelines and on the basis of the permeability and porosity of the weathered rock. Due to the existence of solution-widened joints in the Lake Chesterfield, there can be no guarantees that another sinkhole will not form somewhere within or adjacent to the lake. To reduce the risk of leaks in the future, using reinforced polyethylene (RPE) liners, ethylene propylene diene monomer (EPDM) liners, or polyvinyl chloride (PVC) liners instead of clay liners may be add into consideration.

APPENDIX A.

ERT PROFILES 1-7 AND A-E WITH INTERPRETATIONS

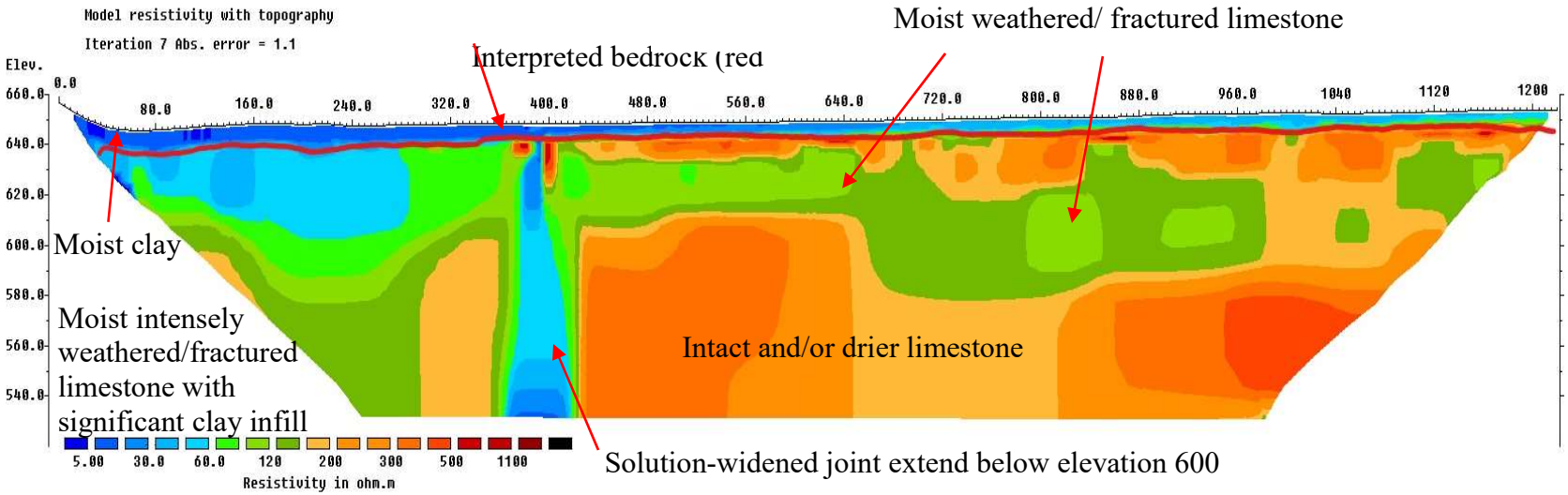

Figure A 1. ERT profile 1 with top of rock marked. Solution-widened joint can be identified near station 400.

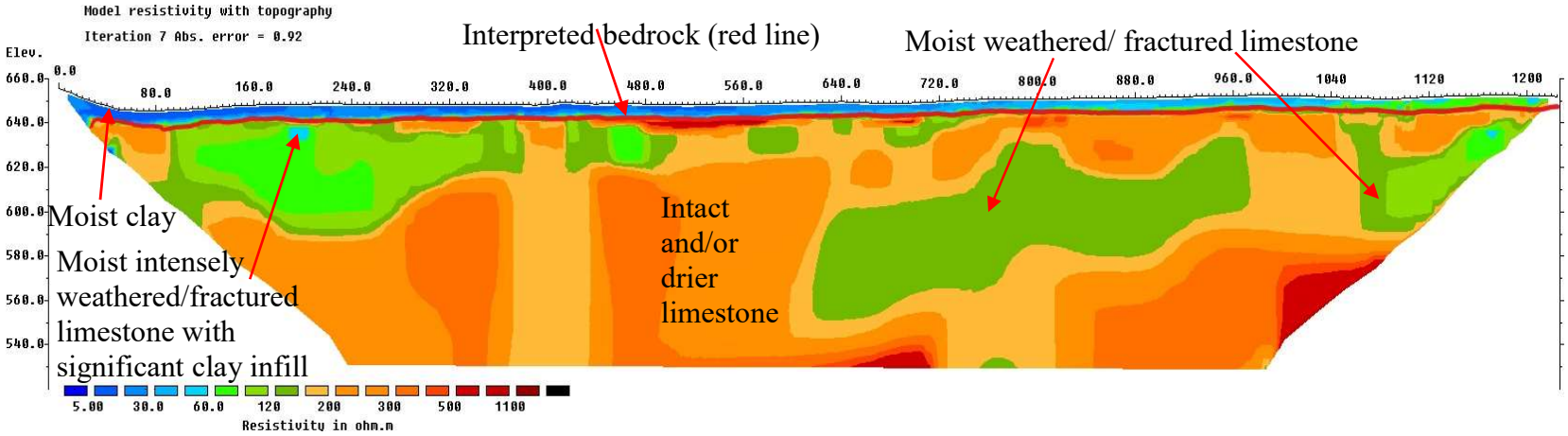

Figure A 2. ERT profile 2 with top of rock marked. The interpreted top of rock correlated well with the 45 ohm.m contour interval.

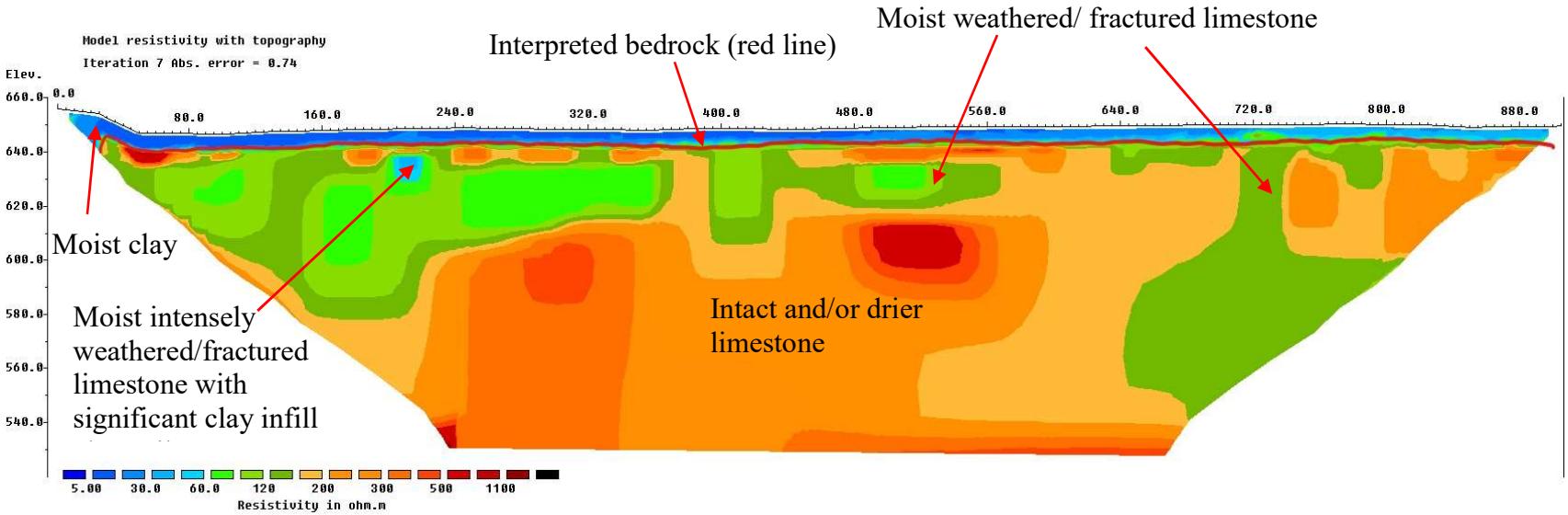

Figure A 3. ERT profile 3 with top of rock marked. The interpreted top of rock correlated well with the 45 ohm-m contour interval.

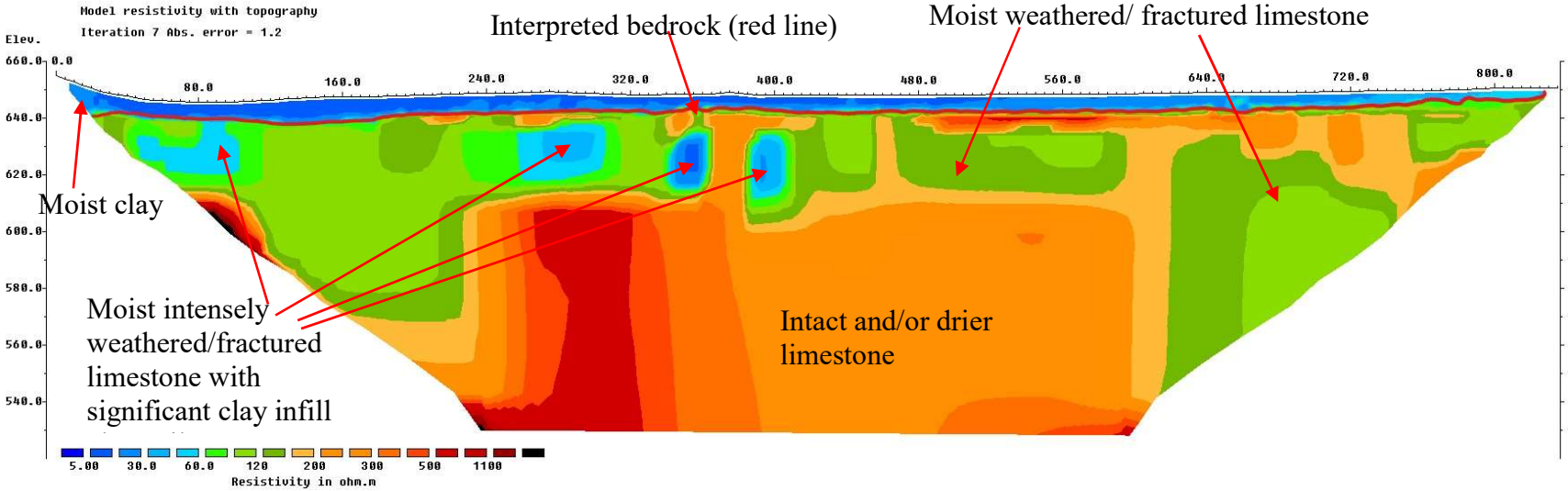

Figure A 4. ERT profile 4 with top of rock marked. The interpreted top of rock correlated well with the 45 ohm-m contour interval.

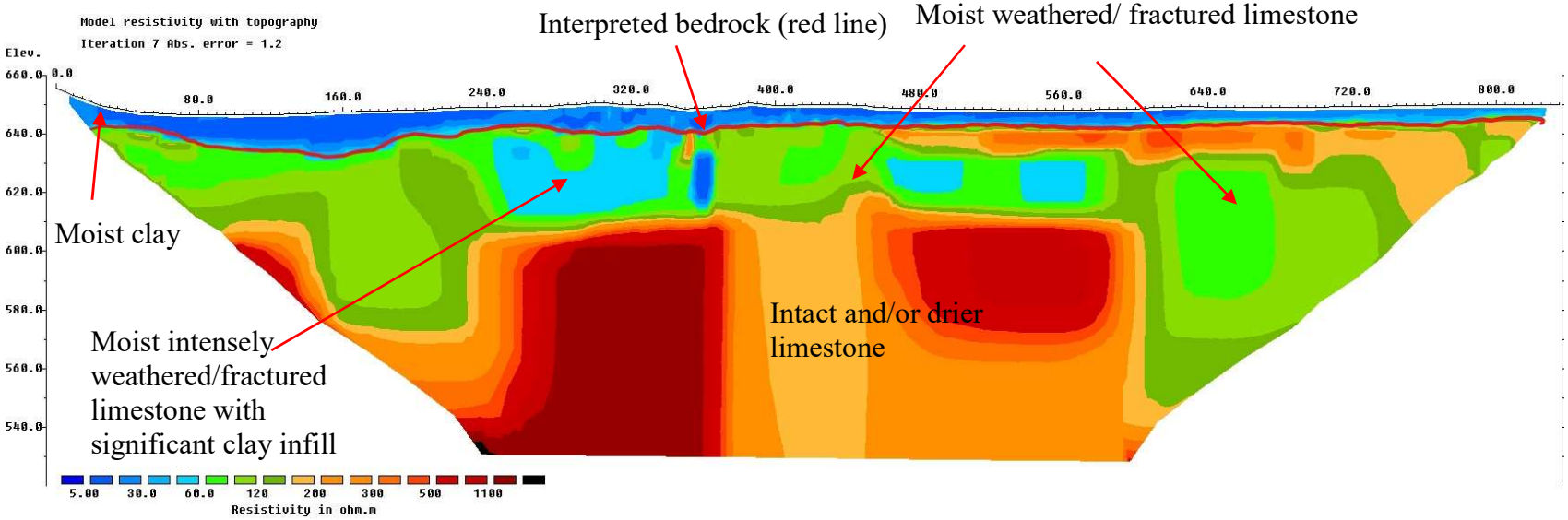

Figure A 5. ERT profile 5 with top of rock marked. The interpreted top of rock correlated well with the 45 ohm-m contour interval.

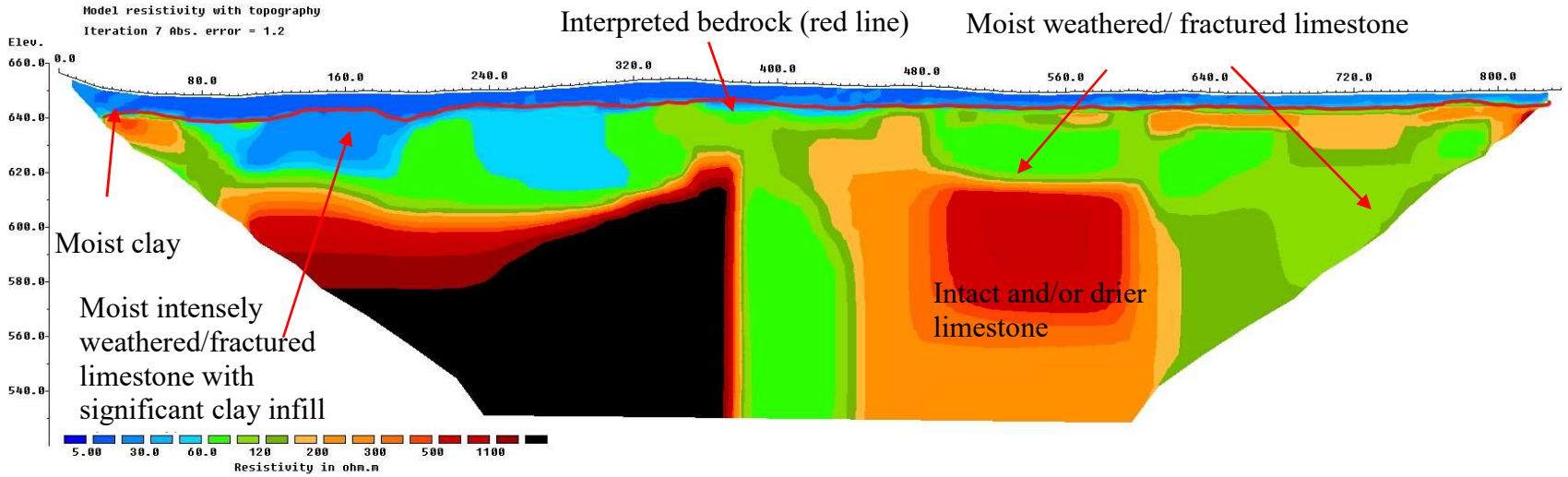

Figure A 6. ERT profile 6 with top of rock marked. The interpreted top of rock correlated well with the 45 ohm-m contour interval.

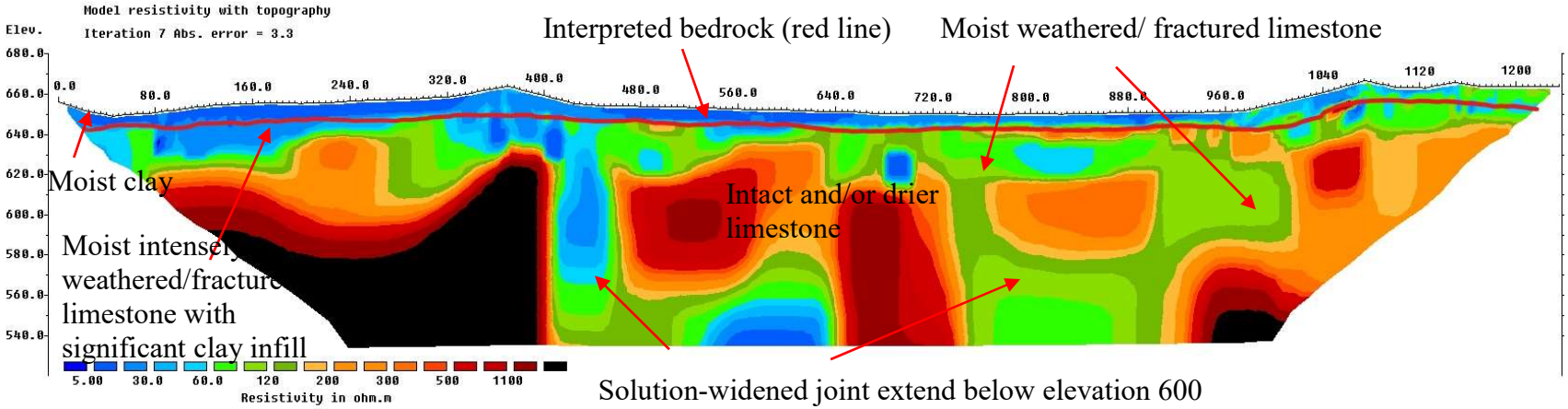

Figure A 7. ERT profile 7 with top of rock marked. Solution-widened joints can be identified near station 440, 740, and 900.

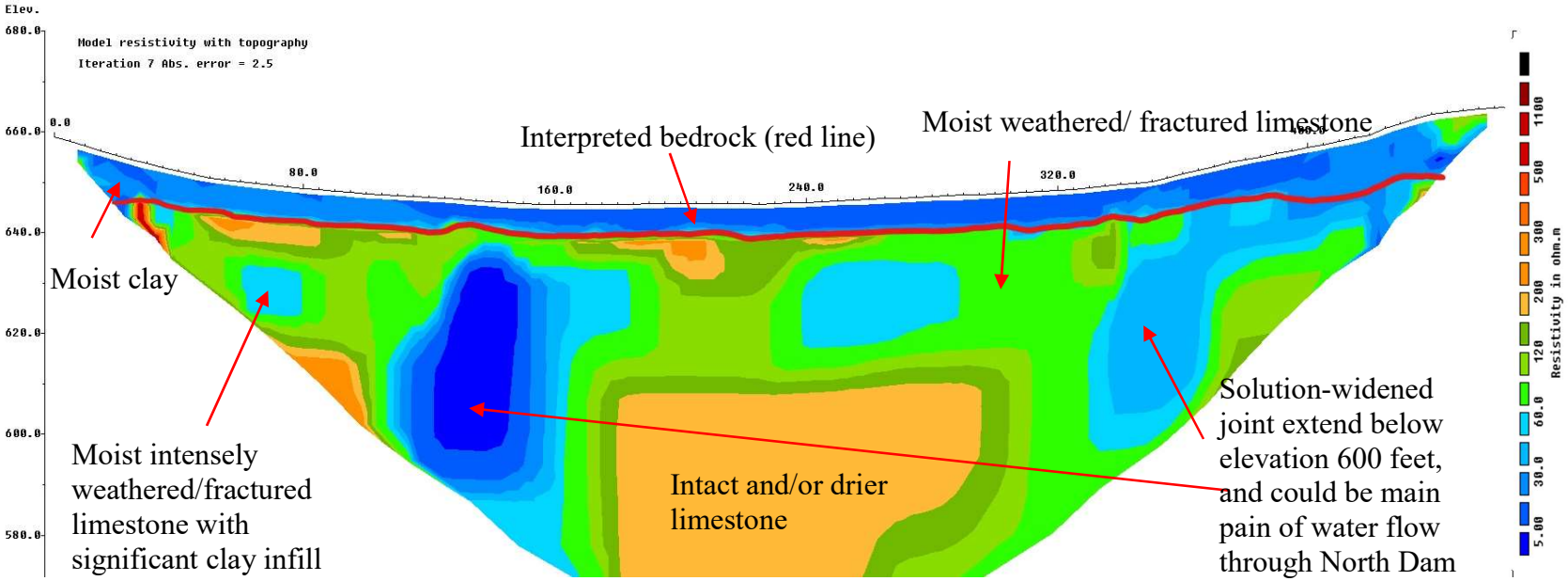

Figure A 8. ERT profile A with top of rock marked. Solution-widened joints can be identified near station 140 and 400.

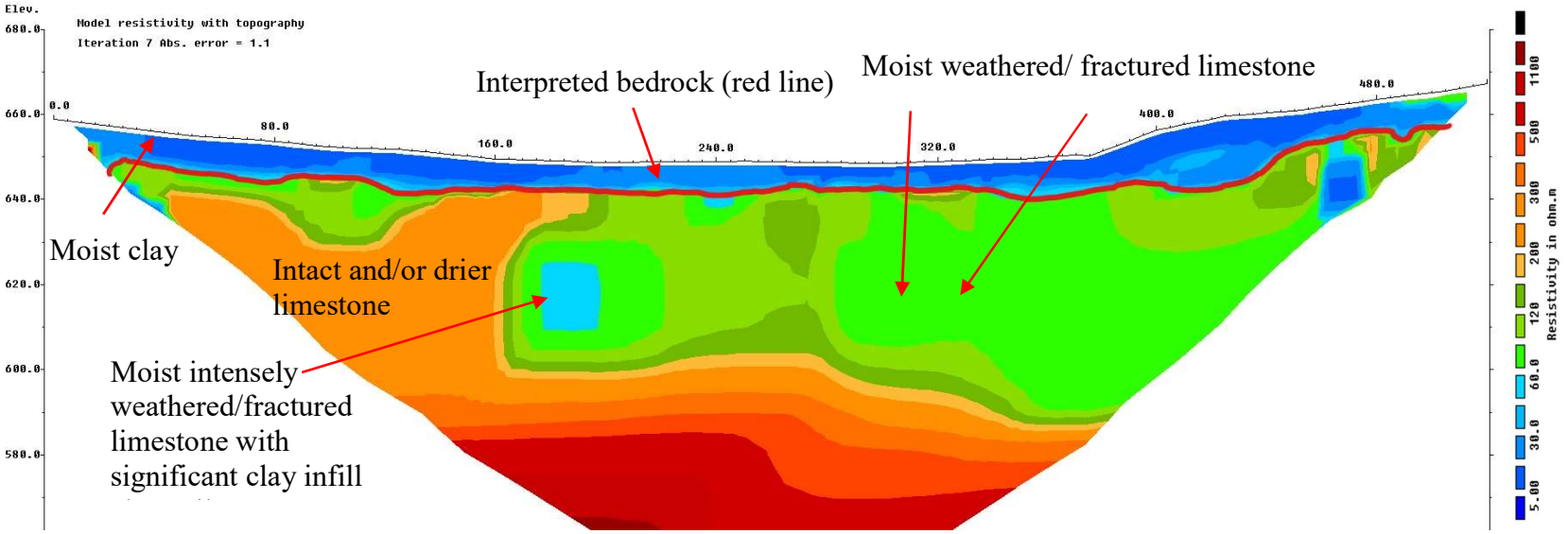

Figure A 9. ERT profile B with top of rock marked. The interpreted top of rock correlated well with the 45 ohm-m contour interval.

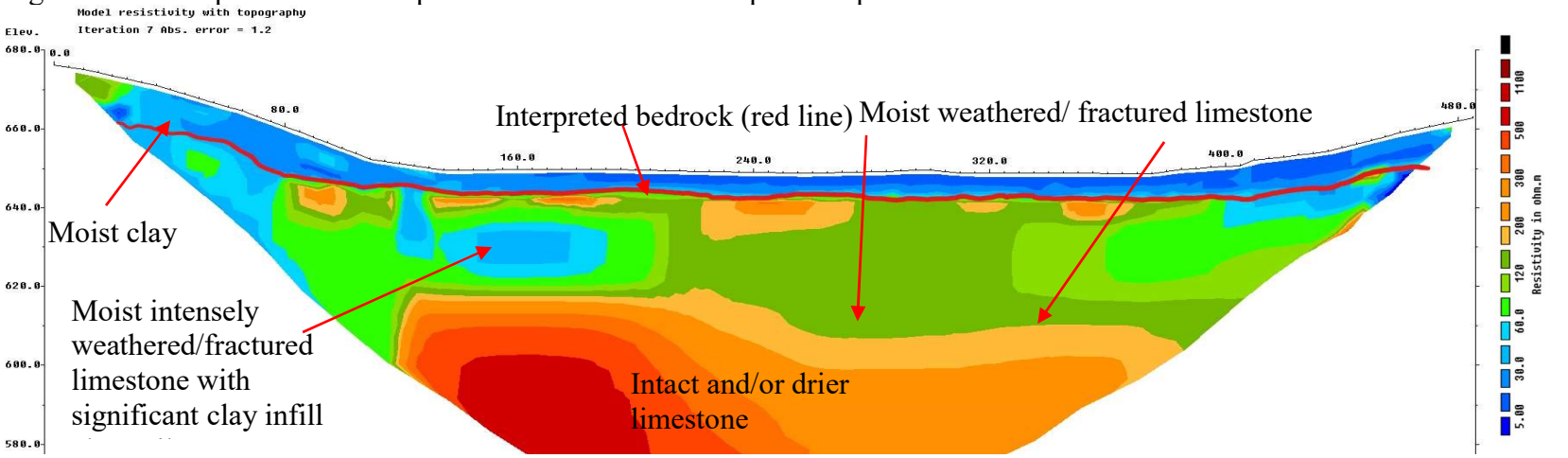

Figure A 10. ERT profile C with top of rock marked. The interpreted top of rock correlated well with the 45 ohm-m contour interval.

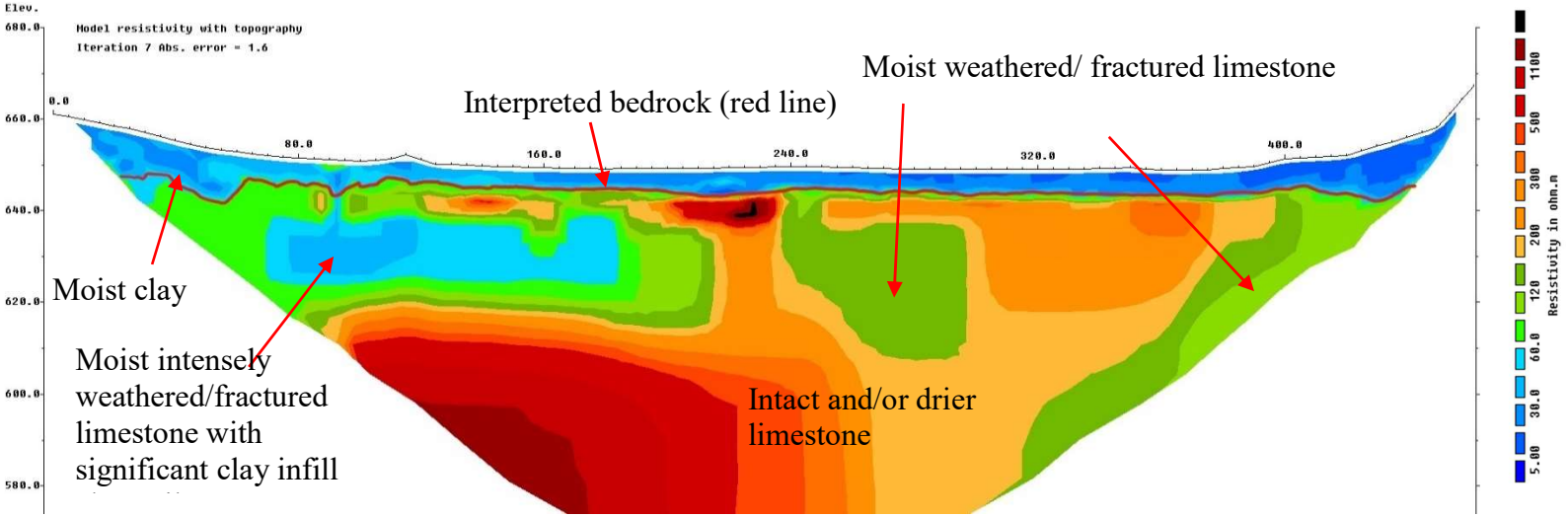

Figure A 11. ERT profile D with top of rock marked. The interpreted top of rock correlated well with the 45 ohm-m contour interval.

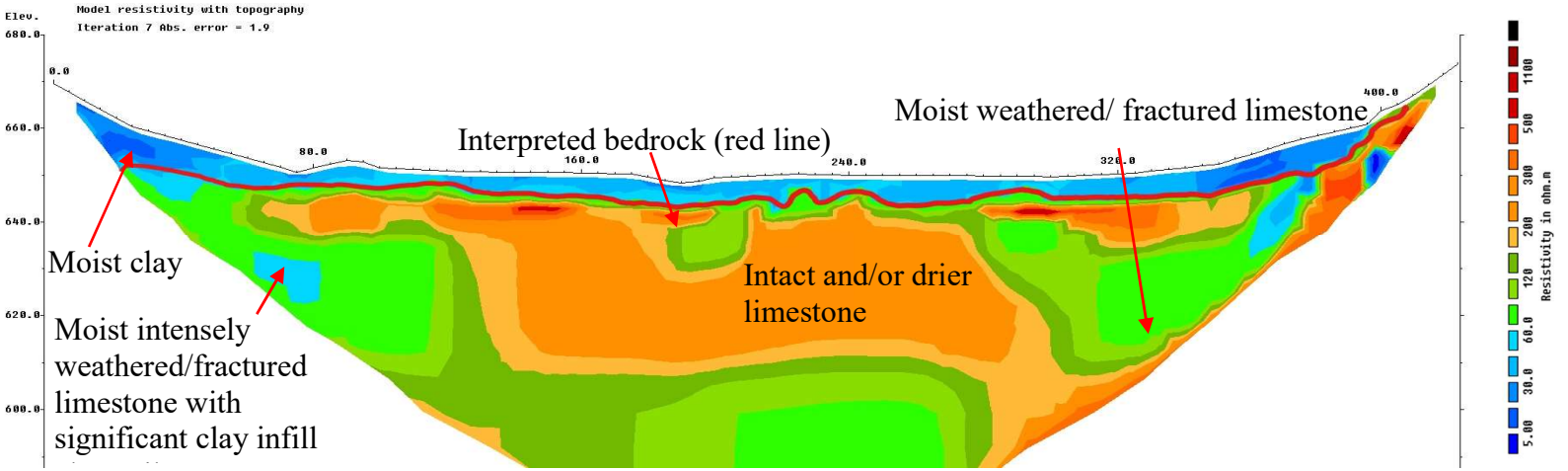

Figure A 12. ERT profile E with top of rock marked. The interpreted top of rock correlated well with the 45 ohm-m contour interval.

APPENDIX B.

MASW PROFILES 1-5 WITH INTERPRETATIONS

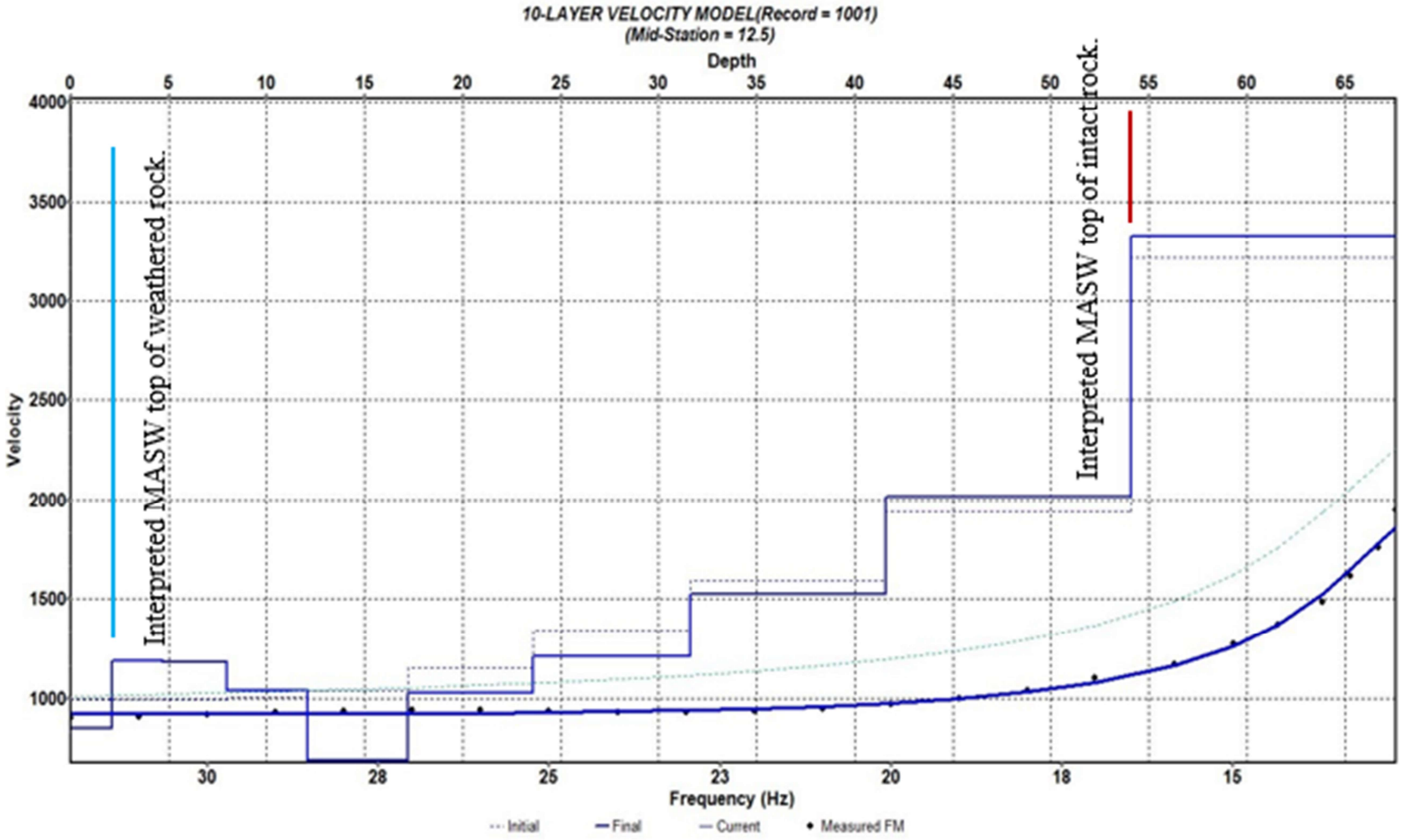

Figure B 1. 1-D shear-wave velocity profile generated for the MASW 1.

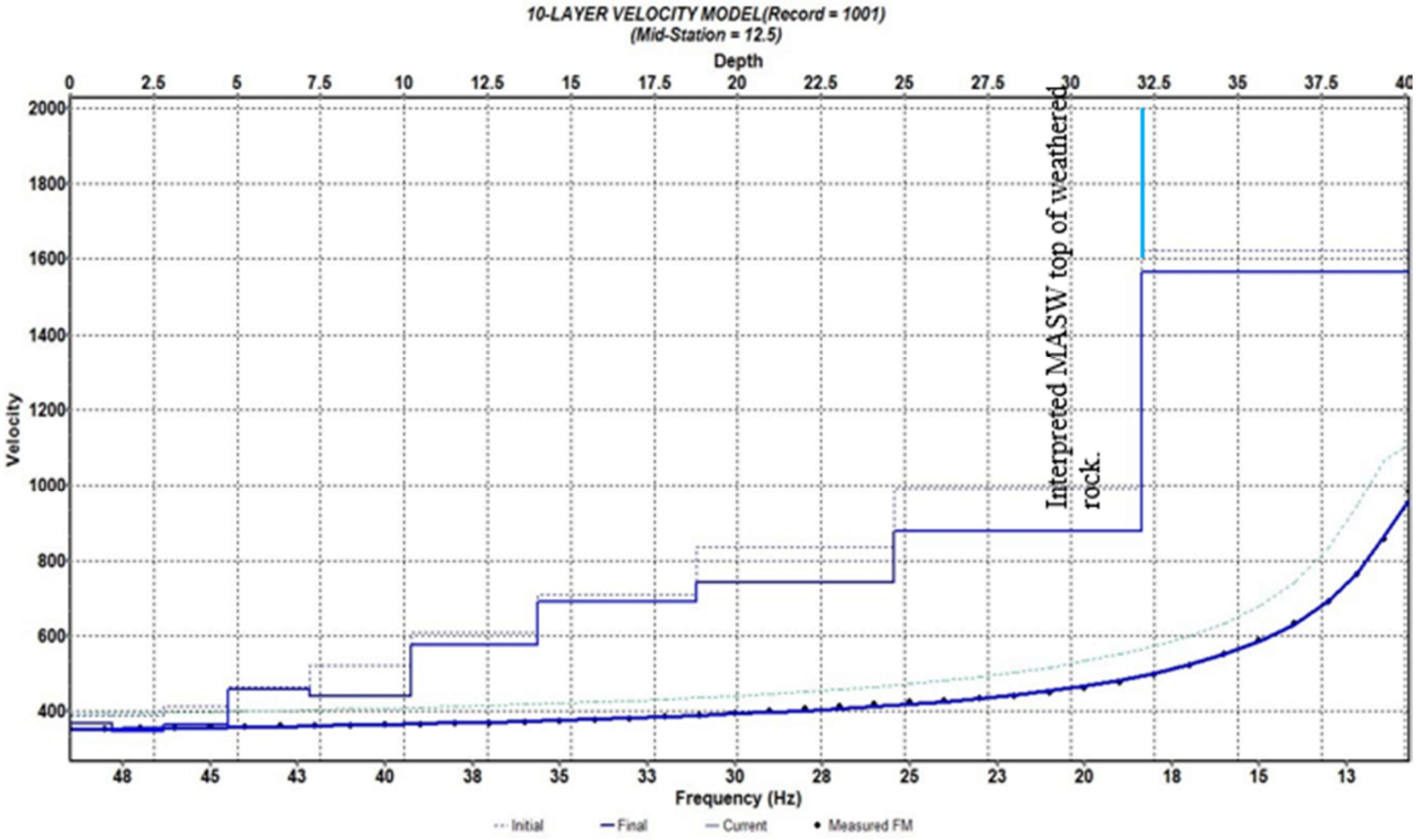

Figure B 2. 1-D shear-wave velocity profile generated for the MASW 2.

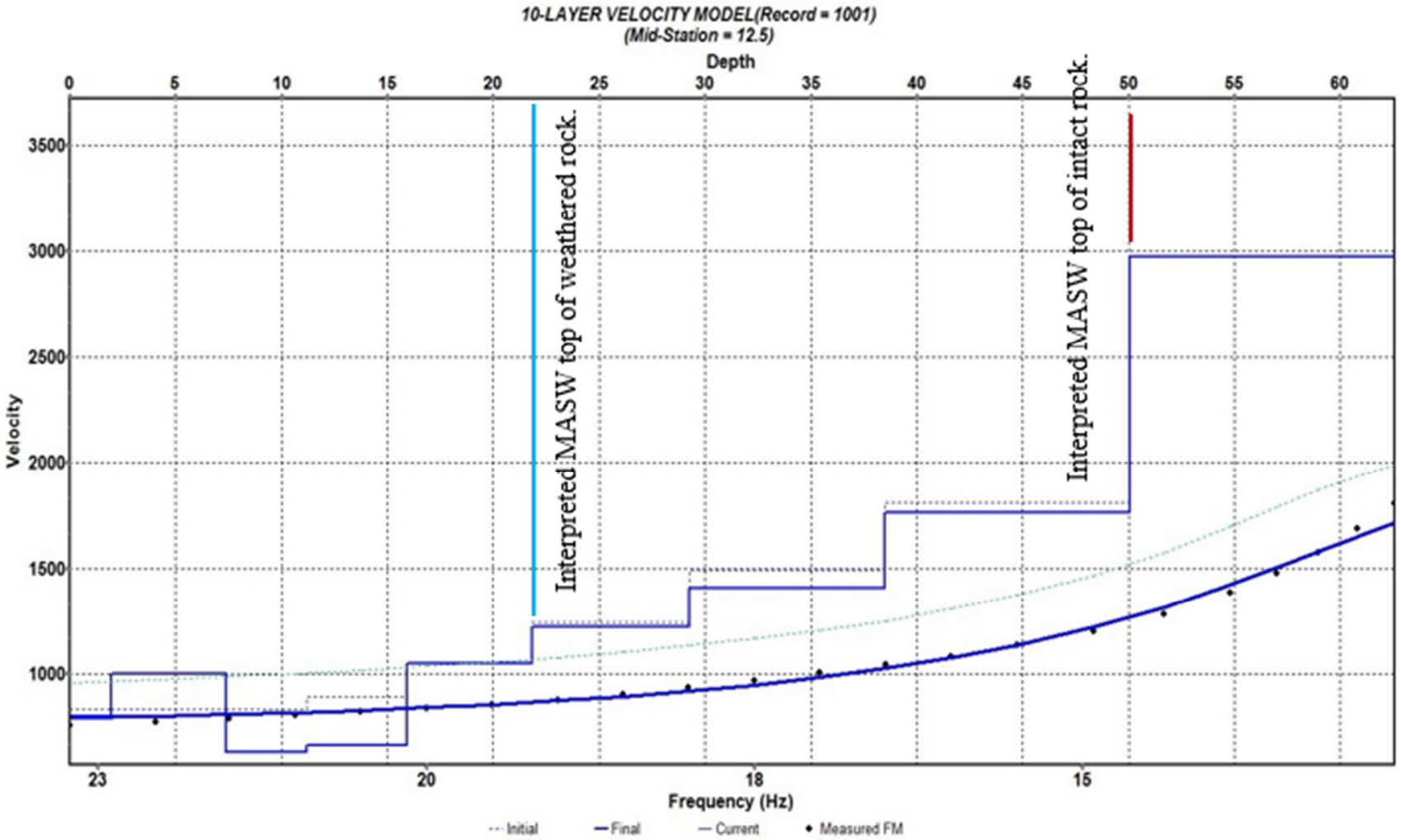

Figure B 3. 1-D shear-wave velocity profile generated for the MASW 3.

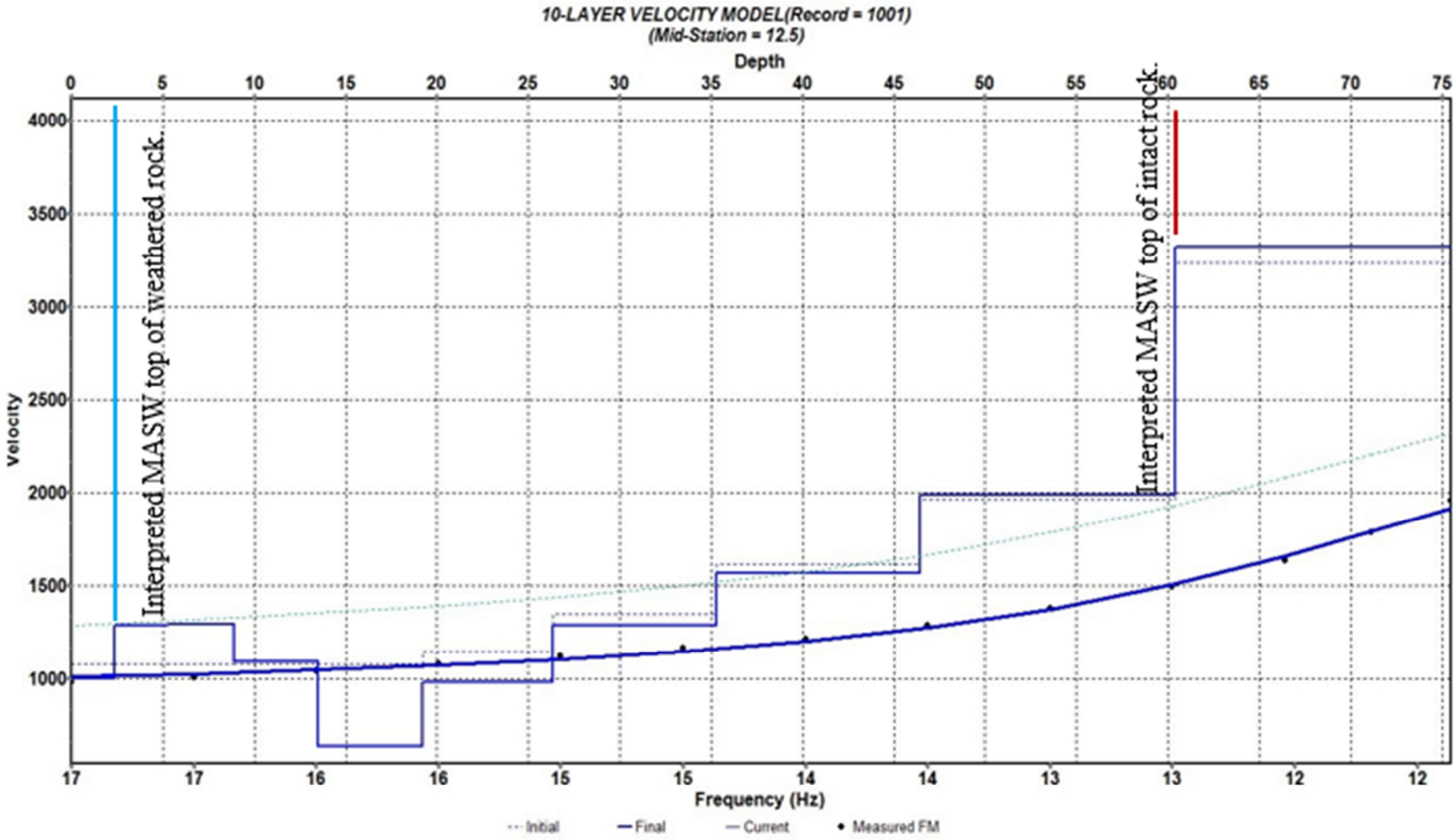

Figure B 4. 1-D shear-wave velocity profile generated for the MASW 4.

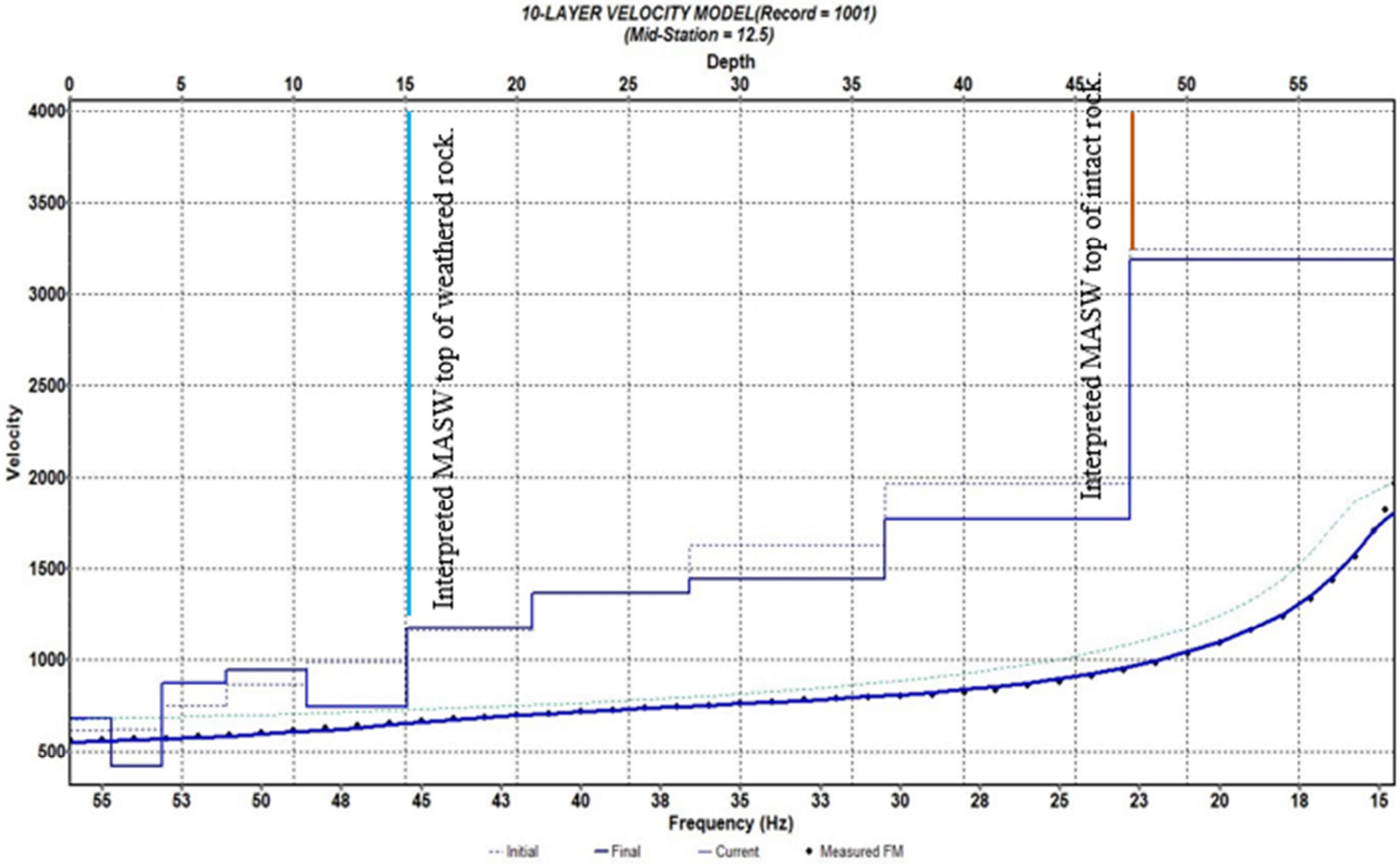

Figure B 5. 1-D shear-wave velocity profile generated for the MASW 5.

BIBLIOGRAPHY

Batayneh, A. T. (2005). 2D electrical imaging of an LNAPL contamination, Al Amiriyya fuel station, Jordan. Journal of Applied Sciences, 5(1), 52-59.

Delgado, A. V., González-Caballero, F., Hunter, R. J., Koopal, L. K., & Lyklema, J. (2005).Measurement and interpretation of electrokinetic phenomena (IUPAC technical report). Pure and Applied Chemistry, 77(10), 1753-1805.

Gercek, H. (2007). Poisson's ratio values for rocks. International Journal of Rock Mechanics and Mining Sciences, 44(1), 1-13.

KGS. (2014, February 3). Introduction to MASW Acquisition and Processing [Painting]. Retrieved from http://www.kgs.ku.edu/software/surfseis/masw.html

Lee, W. H., Jennings, P., Kisslinger, C., & Kanamori, H. (Eds.). (2002). International handbook of earthquake & engineering seismology. Elsevier.

Loke, M.H. (2004) Tutorial: 2-D and 3-D Electrical Imaging Surveys. Geotomo Software, Res2dinv 3.5 Software.

Luo, Y., Xia, J., Miller, R. D., Xu, Y., Liu, J., & Liu, Q. (2008). Rayleigh-wave dispersive energy imaging using a high-resolution linear Radon transform. Pure and Applied Geophysics, 165(5), 903-922.

MacIntyre. (n.d.) Review of MASW and Refraction Surveys. https://www.osop.com.pa/wp-content/uploads/2013/09/masw-remi-survey-guide.pdf

Park, C. B., Miller, R. D., & Xia, J. (1998). Imaging dispersion curves of surface waves on multi-channel record. In SEG Technical Program Expanded Abstracts 1998 (pp. 1377-1380). Society of Exploration Geophysicists.

Renner, T. (2007). Quantities, units and symbols in physical chemistry. Royal Society of Chemistry.

Missouri Department of Natural Resources (2018). Sinkholes in Missouri. [Photograph] Retrieved from https://dnr.mo.gov/geology/geosrv/envgeo/sinkholes.htm

Missouri Department of Natural Resources (2018). Geologic well-St. Louis. [Photograph] Retrieved from https://dnr.mo.gov/geology/wrc/logmain/st_louis.pdf

Thitimakorn, T., & Anderson, N. L. (2004). A 2-D MASW shear-wave velocity profile along a test segment of Interstate I-70, St. Louis, Missouri. In 2006 Proceedings of the Highway Geophysics NDE Conference (pp. 594-608).

United States Geological Survey (2018). The USGS Water Science School. [photograph]. Retrieved from https://water.usgs.gov/edu/sinkholes.html

Weary, D. J., & Doctor, D. H. (2014). Karst in the United States: A digital map compilation and database. US Department of the Interior, US Geological Survey.

Zhou, W., Beck, B. F., & Adams, A. L. (2002). Effective electrode array in mapping karst hazards in electrical resistivity tomography. Environmental geology, 42(8), 922-928.

VITA

Jiawei Li was born in Daqing, Heilongjiang, China on June 1995. In December 2017, he received his BS degree in Geology and Geophysics from Missouri University of Science and Technology in Rolla, Missouri, US. In 2018 he received his second BS degree in Geophysics from Northeast Petroleum University in Daqing, Heilongjiang, China.

In January 2018, he received admission to study geological engineering (M.S) at Missouri University of Science and Technology in Rolla, Missouri, US. He received his Master of Science in Geological Engineering from Missouri University of Science and Technology in December 2018.